PPPL-2266
UC20-G

M.L.L.

(1)

35

DR-0031-0

PPPL-2266

PROPAGATION OF A NONRELATIVISTIC ELECTRON BEAM IN A PLASMA IN A MAGNETIC FIELD

By

H. Okuda, R. Horton, M. Ono, and M. Ashour-Abdalla

OCTOBER 1986

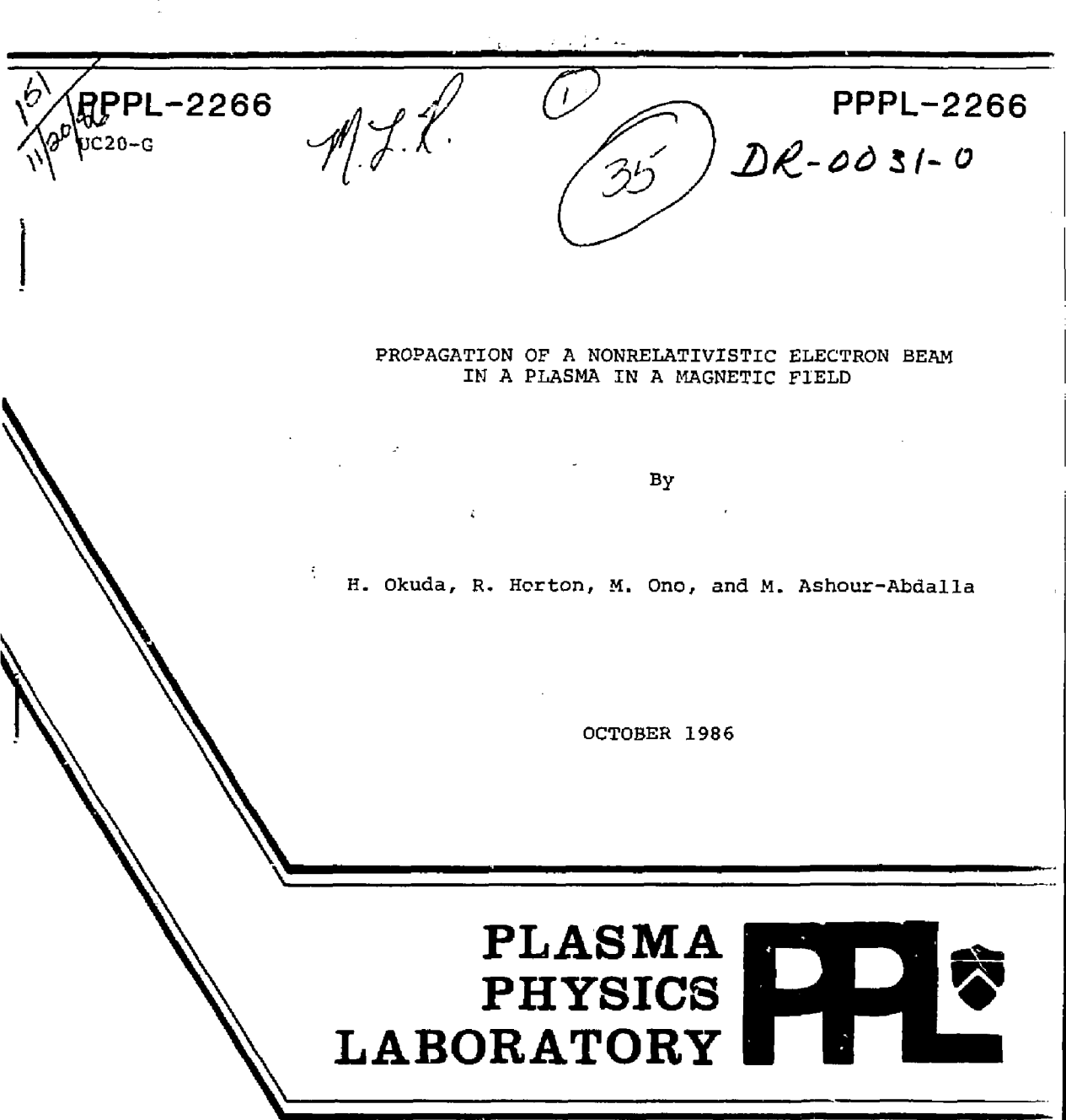

PRINCETON UNIVERSITY
PRINCETON, NEW JERSEY

PREPARED FOR THE U.S. DEPARTMENT OF ENERGY,
UNDER CONTRACT DE-AC02-76-CHO-3073.

PPPL--2266

DE87 002366

PROPAGATION OF A NONRELATIVISTIC ELECTRON BEAM IN A PLASMA IN A MAGNETIC FIELD

H. Okuda, R. Horton, and M. Ono

Plasma Physics Laboratory, Princeton University

P. O. Box 451

Princeton, New Jersey 08544

and

M. Ashour-Abdalla

Institute of Geophysics and Planetary Physics and Department of Physics

University of California, Los Angeles, CA 90024

ABSTRACT

Propagation of a nonrelativistic electron beam in a plasma in a strong magnetic field has been studied using electrostatic one-dimensional particle simulation models. Electron beams of finite pulse length and of continuous injection are followed in time to study the effects of beam-plasma interaction on the beam propagation. For the case of pulsed beam propagation, it is found that the beam distribution rapidly spreads in velocity space generating a plateaulike distribution with a high energy tail extending beyond the initial beam velocity. This rapid diffusion takes place within several amplification lengths of the beam plasma instability given by $(\omega_p \omega_b^2)^{-1/3} V_o$ where ω_p, ω_b, and V_o are the target plasma, beam plasma frequencies, and the beam drift speed, respectively. This plateaulike distribution, however, becomes unstable as the high energy tail electrons free-stream, generating a secondary beam. A

similar process is observed to take place for the case of continuous beam injection when the beam density is small compared with the total density $n_b/n_t < 1$. In particular, the electron velocity distribution is found monotonically decreasing in energy having a high energy tail whose energy reaches twice the initial beam energy. Such an electron distribution is also seen in the laboratory experiment and computer simulations performed for a uniform, periodic system. When the beam density is increased so that the beam current exceeds the thermal return current, $en_bV_o \geq en_ev_t$ where n_e and v_t are the density and thermal speed of the ambient electrons. Beam propagation becomes much slower due to the electric field generated by the excess charges associated with the beam electrons. Beam electrons are reflected from the ambient plasma as if they are bouncing off a rigid wall. When the beam velocity is increased holding the beam density constant, simulations show that the beam current can exceed the return current generated by the thermal electrons, en_ev_t, significantly. It is shown that the electric field generated by the beam plasma instability accelerates the ambient electrons opposite to the beam propagation thereby enhancing the return current.

I. INTRODUCTION

Beam-plasma interaction has been investigated both experimentally and theoretically for more than three decades. The linear theory of beam-plasma interaction is well known.[1-3] In the nonlinear regime, both quasilinear theory[4-6] and single wave nonlinear theory[7-11] are quite well understood. While these nonlinear theories are useful for certain limiting cases, numerical simulations provide rich information in the nonlinear development of the beam-plasma interaction where many modes become nonlinear for both periodic[12-14] and nonperiodic systems.[15-18] These simulations revealed, for example, that trapping of both the beam and background particles is important for particle acceleration and nonlinear saturation when the beam density is not too small.[13,14]

On the experimental side, beam-plasma interaction has been used for plasma production and heating,[19] radiation generation,[17] current drive[14] as well as for active experiment in space.[20]

While most of the laboratory experiments have been carried out in a linear device, recent experiments in a toroidal device[14,21] make it possible to study beam propagation in detail in the presence of beam-plasma interaction. In the current-drive experiment performed in the Advanced Concept Torus-1 (ACT-1) device,[21] a nonrelativistic cold electron beam of a few hundred eV with a density $n_b \lesssim 10^{12}cm^{-3}$ injected from a cathode placed at the bottom of a torus is used to produce a target plasma of ~10 eV and $n_e \lesssim 1 \times 10^{13}cm^{-3}$. The trajectory of the injected beam is primarily controlled by a small vertical magnetic field whose magnitude is an order of a few gauss while the main toroidal field is $B_T \sim 3$ kilogauss.

Measurements of the electron velocity distribution reveal that cold injected beam electrons rapidly evolve into a smooth monotonically decreasing

distribution function with increasing energy. It was found that the energy of tail electrons can reach twice the initial beam energy. Results of plasma simulations using uniform, periodic models[14] show the generation of an electron distribution which resembles very closely that observed in the experiments. It is found that the strong electric field arising from the beam-plasma interaction accelerates both beam and background electrons beyond the initial beam velocity. One of the interesting conclusions from these observations is that the classical mean-free path of such a distribution may be longer than that of the initial cold beam. This is because the high energy electrons generated as a result of beam-plasma instability suffer little slowing down due to Coulomb collisions.[14]

While the results of simulations using the periodic uniform model correctly produce the observed electron distribution in a steady state, physics associated with beam injection and spatial nonuniformity cannot be studied by using such a model. Beam neutralization, spatial amplification of the beam-plasma instability, propagation, and reflection of the beam electrons in space can only be studied using a nonperiodic model.

In this paper, we shall study such a spatially nonuniform system using one-dimensional bounded electrostatic models. In Sec. II, results of simulations for pulsed beam propagation are shown in which a finite length of injected electrons are followed in time to study the interaction with the background plasma. In Sec. III, simulation results are presented in which beam electrons are injected into a plasma at a constant rate in time. Comparisons with the earlier results from periodic simulations and ACT-1 experiments are given in Sec. IV along with further extensions of the study.

II. SIMULATION OF PULSED BEAM PROPAGATION

We shall first study a case in which finite length beam electrons are injected into a plasma. This may correspond to laboratory or space experiments where a short pulsed beam is used. The simulation model uses a one-dimensional electrostatic code with uniform ion background. The time scale of the simulations is therefore essentially the electron time scale which is shorter than the ion time scale. In order to model a pulsed beam, cold beam electrons are placed at the left boundary of the simulation system for $0 \leq x \leq L_b$ where L_b is a small fraction of the total length of the system, L. Charge neutrality is assumed initially so that $n_b + n_e \equiv n_t$ is taken equal to the uniform ion density. Here n_b and n_e are the beam electron and background electron number densities.

The boundary conditions for the electric field and particles are the following. At the far right of the beam electrons no electric field exists since no beam electrons have reached there. Therefore $E(x = L) = 0$ which is sufficient to determine E everywhere in a one-dimensional model. As for particles, background electrons are reflected both at the $x = 0$ and $x = L$ boundaries which equates the particle flux at the right of the boundary to that at the left of the boundary. Note the boundary at $x = L$ is for numerical computations and is not a physical boundary. The absence of net particle flux at $x = L$ guarantees that the plasma remains homogeneous as if there is no boundary. When the beam particles reach the right boundary at $x = L$, the calculation is stopped. A similar model was used for a study of electron transport in laser fusion studies.[22] As noted earlier,[14] one-dimensional simulations are valid only when the beam transverse dimension d is larger than the wavelength along the beam propagation. This condition is met for a "fat" beam or the early time of beam propagation where the radial extent of the beam

is larger than the propagation distance of the beam. When this condition is not met, obliquely propagating plasma waves become important, which requires a two-dimensional model. The qualitative results, however, are found to remain the same for a uniform model.[14] Note also that the electron motion is approximately one-dimensional in a strongly magnetized plasma such as in the ACT-1 device.

Let us consider the first example (case 1) using the model described. Figure 1 shows the phase-space plots at $\omega_{pe}t$ = 0(a), 30(b), 60(c), and 90(d). Here $\omega_{pe} = (4\pi n_t e^2/m_e)^{1/2}$. The simulation parameters are $L = 10^4\ \lambda_e$, $\lambda_e = \Delta$, $n_e\lambda_e = 40$, $V_o/v_t = 10$, and $n_b/n_t = 1/8$ for $0 \le x \le L_b = 128\Delta$. Here Δ is the spatial grid length, and λ_e is the electron Debye length. Note the background electrons are a Maxwellian distribution while the beam electrons are initially cold. Note the beam length is about a factor of two longer than the wavelength of the most unstable mode given by $2\pi V_o/\omega_{pe} = 62\Delta$. As shown in Fig. 1, the cold beam spreads out completely in velocity space on a very short time scale, $\omega_{pe}t$ = 30 generating vortices characteristic to the motion of trapped particles. The velocity distribution f(v) at $\omega_{pe}t$ = 30 averaged over a short distance in x shows a smooth, plateaulike distribution which is stable against the beam-plasma instability, $f' \lesssim 0$. The energy of the beam electrons reaches twice the initial beam energy, which is consistent with the ACT-1 observations and with earlier simulations.[14]

As the high energy tail electrons stream through the background plasma shown in Fig. 1(c), however, a second phase of beam-plasma instability develops generating a velocity space modulation shown in Figs. 1(c) and 1(d). This secondary phase of the instability is caused by the beam electrons resulting from the free streaming of the plateaulike distribution shown at Fig. 1(b). As the high energy electrons stream faster than the low energy

electrons, a beamlike distribution is generated at the downstream side. The secondary instability generated by the beamlike distribution slows down the high energy particles so that the total distribution again approaches a smooth, plateaulike distribution seen earlier. Such a distribution is destabilized again as the high energy particles stream through the background plasma. By repeating such a process, the electron distribution develops a smooth, monotonically decreasing function of particle energy similar to that observed in the earlier periodic simulation.

The large amplitude waves generated by the initial cold beam and by the secondary instability are clearly shown in Fig. 2 for $\omega_{pe}t$ = 10(a), 30(b), 60(c), and 90(d). Here the normalized electric field ($eE/m_e\Delta\omega_{pe}^2$) is shown. For $\omega_{pe}t \lesssim 30$, a strong instability develops in space as the beam electrons interact with the background electrons. For $\omega_{pe}t$ = 60 and 90, generation of the electric field is accompanied by the free-streaming electrons forming a beam distribution. Such a secondary instability is weaker as evidenced from the smaller amplitude of the electric field at the downstream side shown in (c) and (d).

To confirm generation of beams associated with free-streaming, local velocity distributions are plotted at several different locations in x. Figure 3 shows the instantaneous local velocity distribution at $\omega_{pe}t$ = 90 measured at bin 4 ($384\Delta \le x \le 512\Delta$), (a), bin 5 ($512\Delta \le x \le (640\Delta$), (b), bin 6 ($640\Delta \le x \le 768\Delta$), (c), and bin 7 ($769\Delta \le x \le 896\Delta$, (d). Note the distribution is more or less monotonically decreasing with particle velocity for bin 4. Rapid fluctuations are due to the fact that the velocity distributions are instantaneous without any time averaging. Distinct beamlike features are obvious for bins 5, 6, and 7 which are caused by the free-streaming of the high energy electrons.

When the beam density is increased to n_b/n_t = 1/4 and 1/2 for $0 < x \leq 128\Delta$, a similar process is found to take place. In addition, propagation of the beam electrons toward downstream becomes slower due to the electric field arising from the net local charges as the beam electrons propagate. This is discussed in detail in Sec. III where a continuous beam injection is simulated.

In order to confirm the beam generation and the secondary instability resulting from free-streaming of a plateaulike distribution, a simulation with a Maxwellian distribution for the background and plateaulike distribution for $0 \leq x \leq 128\Delta$ given by

$$f = \begin{cases} n_b & \text{for} \quad 0 < v < V_o \\ 0 & \text{otherwise} \end{cases}$$

is carried out where n_b/n_t = 1/4 and $L = 1024\lambda_e$ (case 2). Initially $f' \leq 0$ everywhere so that the plasma is stable with respect to beam-plasma instability. As the high energy particles from the plateaulike distribution stream through the plasma, a beam-like distribution is generated causing a beam-plasma instability. Figure 4 shows the phase space at $\omega_{pe}t$ = 0(a), 30(b), 60(c), and 90(d). As the high energy particles run away, a velocity space modulation develops at $\omega_{pe}t$ = 30 and develops a large amplitude at $\omega_{pe}t$ = 60. This instability in turn slows down the beam and the distribution spreads in velocity space generating a plateaulike distribution at $\omega_{pe}t$ = 90 for the bulk of the electrons except at the tip which tends to free stream downward.

Figure 5 shows the electric field structure and the local velocity distribution at $\omega_{pe}t = 50$, (a),(b) and at $\omega_{pe}t = 90$, (c),(d). At $\omega_{pe}t = 50$, the waves are localized for $0 \lesssim x \lesssim 400\Delta$ while they spread almost to the entire system at $\omega_{pe}t = 90$. Local distributions measured at bin 4 ($384\Delta \leq x \leq 512\Delta$) at $\omega_{pe}t = 50$ and bin 8 ($896\Delta \leq x \leq 1024\Delta$) at $\omega_{pe}t = 90$ clearly indicate the presence of beams resulting from the streaming of the high energy electrons of the initial plateaulike distribution. It is clear such beam electrons are responsible for generating an electric field as a result of beam-plasma interactions.

III. SIMULATIONS OF BEAM INJECTION AT A CONSTANT RATE

We shall now study the results of beam injection into a plasma at a constant rate in time. The background plasma is initially charge neutral so that the injection of beam electrons produces excess negative charges near the injection point. The plasma is no longer charge neutral and the electric field generated by the excess electrons pushes the background electrons out of the system at $x = 0$, and they are considered lost. The electric field slows down the beam electrons at the same time. Beam electrons leaving the left boundary after reflection are also considered lost. The boundary condition at the right, $x = L$, is the same as the previous model reflecting the target electrons at $x = L$ where $E(x = L) = 0$. Note that there is no net particle flux at $x = L$ so that the plasma remains homogeneous near the right boundary at $x = L$. The reflected particles can be regarded as those coming from the right of the boundary in a homogeneous unbounded plasma. At the left boundary, $x = 0$, cold beam electrons are injected at a constant rate in time such that the beam density is equal to the prescribed fraction of the background density. As mentioned, electrons leaving the left boundary at

$x = 0$ are considered lost. Note $E(x = 0)$ is not equal to zero due to the excess net charges in the system. The electric field is responsible for the slowing down of the incoming beam electrons and at the same time pushes both the background and beam electrons out of the system. There are net charges, however, in this model for $0 \leq x \leq L$ since complete neutralization is not possible.

It should be pointed out that the choice of the electric field at the right boundary, $E(L) = 0$, indicates that no net charge exists for the region for $x < L$ although the plasma region for $0 < x < L$ is generally not charge neutral. This is because if the charge neutrality is not satisfied for $x < L$, then the electric field flux should be finite at $x = L$, $E(L) \neq 0$. The choice of $E(L) = 0$ indicates that, therefore, there is a net charge for $x < 0$ which just cancels the net charge for $0 < x < L$ so that no net charge exists for $x < L$. One such example corresponds to an electron beam injection from a spacecraft. As the beam electrons leave the spacecraft, an equivalent amount of positive charges remain on the spacecraft so that the total charge is always zero.[23]

We should point out the differences of our present model from those in earlier works[15,16] using nonperiodic models for beam-plasma interactions. In both cases the beam density was chosen to be much smaller than the present work. Furthermore, space charge effects due to charge non-neutrality were neglected, which may be valid for a very low density beam.[16] As will be shown, an electric field arising from non-neutral charges plays a very important role in beam propagation and reflection when the beam density is not too small compared with the background density. In addition, the boundary conditions on the electric field, as well as the initial conditions in our model are different from the previous works.[15,16] In the present model, the

electric field is assumed zero far away from the injection point while it is zero at the injection point[15] or it is not zero ahead of the beam.[16] Also, in earlier simulations,[15,16] the initial conditions are taken such that the plasma and beam electrons are neutralized across the entire system so that the beam neutralization process cannot be studied. Needless to say, the boundary condition of the electric field plays an important role in the physics of beam propagation. We should mention that Gauss's equation was solved directly using a spatial grid without using a fast Fourier transform, which works poorly in the presence of sharp discontinuities. Also, a sufficiently small time step Δt, $V_o \Delta t \ll \Delta$ must be used for maintaining the accuracy of the simulations.

With the model mentioned, simulations are carried out using the same parameters as in case 1 where $n_b/n_t = 1/8$ and $V_o/v_t = 10$ (case 3). Note that the beam current en_bV_o is approximately equal to the thermal current en_ev_t for this case. Figure 6 shows the electric field (a), target electron density (b), phase space for the beam electrons (c), and the phase space for the target electrons (d) at $\omega_{pe}t = 10$. In order to show the spatial structure in more detail, only a quarter of the system length is shown in Fig. 6 ($L = 256\lambda_e$). Note the electric field at $x = 0$ is positive at this instant which repels the beam and background electrons to the left. Large electron density modulation is induced as shown in (b). The tip of the beam electrons manages to propagate into a plasma at roughly the initial velocity as shown in (c). This is because the plasma cannot respond to the beam instantly. In fact, it takes $t \sim \omega_{pe}^{-1}$ for the plasma to respond to the incoming particles. As the electric field is built up to stop the beam electrons, beam electron are cramped near $x = 50\Delta$. The phase space of the ambient electrons, shown in (d), indicates a modulation whose wavelength is given by $2\pi V_o/\omega_{pe}$.

At $\omega_{pe}t$ = 20, the amplitude of the beam-plasma instability increases further, generating vortex structure in the phase space of the electrons shown in Figs. 7 (c) and (d). Both the electric field (a) and the ambient electron density (b) indicate a coherent wave structure propagating to the right. The beam electrons are found to be trapped coherently in phase space as shown in (c) because they are resonant with the wave. A coherent vortex structure is also seen in the background electrons, (d), similar to the earlier periodic simulations.[14]

The wavelength of the coherent structure roughly corresponds to the most unstable mode given by $\lambda \approx 2\pi V_o/\omega_{pe}$ as shown in (a). Note the presence of a very sharp density spike in (b).

At a later time, $\omega_{pe}t$ = 50, shown in Fig. 8, the instability propagates towards the right at roughly the original beam speed even though the beam electrons spread out in velocity space as shown in (c). Here in Fig. 8, the total length of the system $L = 1024\lambda_e$ is shown. The phase space of the background electrons (d) develops a vortex structure with the wavelength corresponding to the most unstable mode. Note the maximum energy of the beam and background electrons reach nearly twice the initial beam energy in agreement with the previous periodic simulations of a homogeneous plasma.[14]

At $\omega_{pe}t$ = 100, shown in Fig. 9, the beam electrons fill the entire simulation system so that the computing is stopped at this time. While there are coherent structures observable in the beam and the ambient electron phase space, significant thermalization via coalescence has developed. Beam particles are gradually thermalized in velocity space as they propagate further into the ambient plasma. The phase-space distribution and the amplitude of the beam-plasma instability at this time are very close to the previous results obtained from periodic uniform simulations.[14]

The simulation results are also consistent with the observations of the electron distributions measured in the ACT-1 device, which indicate a presence of very rapid diffusion of beam electrons in velocity space. Cold beam particles at the cathode are found to evolve into a smooth, monotonically decreasing velocity distribution within a short distance from the cathode plate.

Such a thermalization of the beam and ambient particles via coalescence to a smooth, monotonically decreasing distribution is clearly seen in the present simulation in which beam and ambient electrons undergo thermalization caused by a beam-plasma instability, as shown in Figs. 6, 7, 8, and 9. The convective amplification length defined by $(\omega_p \omega_b^2)^{-1/3} v_o \approx 20\Delta$ is very short so that it takes only a few amplification lengths for the electric field to develop to a large amplitude thereby accelerating both the beam and the ambient electrons significantly. Gradual coalescence of vortices produces a smoother electron velocity distribution. These observations are quite similar to the earlier results obtained for the periodic system.[14]

Figure 10 shows the total electron distribution at $\omega_{pe}t = 80$ including both beam and background electrons averaged over the entire system length. We see a smooth, monotonically decreasing high energy tail extending beyond the initial beam energy at $V_o = 10\ v_t$ by a factor less than 2, which is in good agreement with the ACT-1 observation. As discussed these high energy particles are produced as a result of trapping and subsequent thermalization.

Figure 11 shows the single point measurement at $x = 512\Delta$ of the power spectrum of the electric field. The electric field grows in time saturating at $\omega_{pe}t = 100$. The frequency is completely dominated by the beam-plasma interaction in which the frequency of the most unstable mode lies just below ω_{pe}.

When the beam current is reduced below the thermal current of the target plasma given by $en_e v_t$, beam electrons can propagate freely into the target plasma. Figure 12 shows the phase space of beam electrons, (a), (c) and target electrons, (b), (d) at $\omega_{pe}t$ = 50 and 100. The parameters of the simulation are the same as the previous case 3 except that the beam density is reduced to n_b/n_t = 0.0675 keeping the beam velocity at V_o/v_t = 10 (case 4). Here the system length L is equal to 1024Δ. Trapping and diffusion of beam particles cause acceleration, resulting in the production of a high energy tail as before. The vortex structure on the ambient electrons accelerates these electrons comparable to the beam particles, resulting in a diffusion in velocity space. Overall though, the beam electrons propagate into the target plasma at roughly the initial injection speed. Since the beam current is small in this case, beam neutralization should not be a problem. In the following we shall study a case where the beam current exceeds the thermal current of the ambient plasma.

When the beam density is increased to 25% of the target density so that $en_b V_o \approx 3en_e v_t$, qualitatively different physics emerges. Using the same parameters as before except for n_b/n_t = 0.25, Figs. 13 and 14 are obtained (case 5). L = 512Δ is chosen. At $\omega_{pe}t$ = 10 shown in Fig. 13, the initial development for this case is similar to Fig. 6 for n_b/n_t = 0.125 (case 3). The target electrons, Fig. 13(b), are pushed out to the left due to the beam electrons, Fig. 13(c), which are cramped together except for the tip which free streams as before. Note that some of the beam and the target electrons are reflected back due to the strong electric field, as shown in phase space, Figs. 13(c) and (d). The target electron density, Fig. 13(b), shows a presence of a hole due to the incoming beam electrons. They are pushed out of the plasma to the left.

As time goes on, instead of exciting the plasma oscillations, which took place for a low density beam, a quasistatic pressure balance persists between target and beam electrons as shown in Fig. 14 at $\omega_{pe}t = 50$. The density depression of the target electrons expands to the right, (b), while the electric field slows down the beam electrons (c). It is interesting to observe in (c) that the beam electrons are decelerated to a velocity much smaller than the injection velocity as they propagate into the plasma. Since the beam density is sufficiently high in this example, the net negative charge at the boundary of the beam and target electrons is more than just a small perturbation. The electric field generated is strong enough to trap and slow down the beam electrons except for the tip of the beam which can penetrate into a plasma without attenuation and form precursor electrons. Apparently this process did not occur for a lower beam density as the electric field was not large enough to excite plasma oscillations (cases 3 and 4). In an actual beam propagation experiment, the radial electric field caused by the finite transverse dimension of a beam may cause a radial spread. Note the radial spread is not allowed in a one-dimensional model which may be justified for a beam propagation in a strong magnetic field. The target electrons develop one single vortex structure in phase space, (d). At a much later time, $\omega_{pe}t = 100$, the vortex structure moves slowly downstream at a speed much smaller than the beam injection speed. While the tip of the beam electrons free streams, the bulk of the electrons are trapped and slowed down in the form of a single vortex structure. The vortex structure persists for a long time, more than several hundred plasma oscillations, which moves slowly toward the downstream side at a speed slightly smaller than the thermal speed of the ambient electrons. The propagation speed is therefore much smaller than the initial beam velocity and the process is more like a thermal expansion. This result

is very different from the previous case when the beam density was lower so that the electric field was smaller. As the beam electrons come in, an oscillating electric field is set up so that the average force on the beam electrons more or less vanishes leaving them to propagate freely along the downstream side. When the beam density is higher, such as in this case 5, the electric field is so strong and the average force does not vanish. Most of the beam electrons are essentially cramped at the injection point which then slowly expand downstream at a speed of the order of the thermal speed.

When the beam density is further increased to 50% of the target density, reflection of beam electrons becomes more apparent (case 6). Figure 15 shows the total velocity distribution at $\omega_{pe}t = 20$ (a), and 50 (b), and beam phase-space plots at $\omega_{pe}t = 20$ (c) and 50 (d). Here $L = 510\Delta$ is taken. It is apparent that the two peaks at $v = 0$ and $v = -10\ v_t$ correspond to the target and reflected beam electrons. The beam phase-space plot at $\omega_{pe}t = 20$ shows the cramped beam electrons clearly. It is clear that the electrostatic repulsion is so strong in this case that most of the beam electrons are reflected at the injection point as if they are bouncing off a rigid wall, except for the tip of the beam which forms precursor electrons. Only a small fraction of beam electrons manages to propagate at a speed much less than the injection speed.

We shall now study the propagation of an electron beam in which the beam current exceeds the thermal current by increasing the beam injection speed, thereby increasing the beam energy.

Figure 16 shows the beam propagation for the case of $n_b/n_t = 1/8$ and $v_o/v_t = 20$ (case 7) so that $en_bV_o \approx 3\ en_ev_t$. Electric field (a), ambient electron density (b), beam phase space (c), and ambient phase space (d) at $\omega_{pe}t = 25$ are shown. It is interesting to observe that the beam particles can

propagate in the ambient plasma freely despite the fact that the beam current is more than twice the thermal current. Note the wavelength of the modulation due to beam-plasma interaction is longer than that for the previous examples where $V_o/v_t = 10$ was used (cases 3,4). This is because the most unstable wave number is given by $k^{-1} = V_o/\omega_{pe}$.

At time $\omega_{pe}t = 50$, shown in Fig. 17, we observe the trapping of the beam particles and vortex structure in phase space. Note the propagation speed is roughly equal to but slightly smaller than the initial beam speed.

It is very interesting to find out that the beam is able to propagate even at a higher drift speed. Figure 18 shows the phase space plots for beam (a), (c), and ambient electrons (b), (d) at $\omega_{pe}t = 25$ and 50. The simulation parameters are $L = 2048\lambda_e$, $V_o/v_t = 40$, and $n_b/n_t = 1/8$ so that $en_bV_o \approx 6\ en_ev_t$ (case 8). Propagation speed is slower than the free streaming, though it is not much smaller than V_o. By examining the ambient electron phase space, Figs. 18(b) and (d), we note the ambient electrons are accelerated toward the beam injection point at $x = 0$ indicating the beam current is balanced by the increased return current carried by the target electrons. The same phenomenon is observed in Figs. 16(d) and Fig. 17(b) where the enhanced flow of the ambient electrons toward the cathode plate is generated. Such a current is generated by an electric field caused by the beam-plasma instability.[23]

IV. DISCUSSION

Propagation of beam electrons has been studied by using one-dimensional electrostatic particle simulation models with appropriate boundary conditions for particles and fields. For the case of constant injection of beam particles, it is found that the beam electrons can propagate freely into an

ambient plasma only when the density is smaller than the ambient density. Simulations with $n_b/n_t = 0.125$ show good agreement with the experimental data from ACT-1, which also agrees well with the homogeneous, periodic simulations. When the beam density approaches the ambient density so that the beam current en_bV_o exceeds the thermal current given by en_ev_t, it is found that most of the beam electrons are reflected by the electric field generated by the beam electrons. In this case, the electric field generated by the excess charges of the beam electrons exert a net force on the electrons causing slowing down and reflection of the beam and the ambient electrons. When the current is increased by increasing the beam drift speed, it is found that the beam current can exceed the thermal current. This enhanced return current carried by the ambient electrons is generated by the electric field caused by the beam-plasma instability.

While the simulation model is one-dimensional, actual beams have a finite transverse dimension. When the plasma is strongly magnetized, such as in the ACT-1 device, motion across the magnetic field is prohibited so that the motion of the electrons is one-dimensional. In this case, the one-dimensional model is appropriate provided the waves generated are also nearly one-dimensional. In the presence of a radial electric field, electrons rotate by the $c\underline{E} \times \underline{B}/B^2$ drift around the magnetic field which may be responsible for the stability of the beam electrons as well as beam diffusion across the magnetic field. Such effects can only be studied by using a two-dimensional model.[24]

While the simulation results agree well with the ACT-1 experimental results at low beam current, no experimental data are available at higher current in the ACT-1 device. Recent data from a space shuttle experiment on electron beam injection indicate several interesting physical processes, including space shuttle charging, beam propagation, and wave generation.[25]

While no detailed data from space shuttle experiments are available yet, there are indications that the beam electrons are reflected back to the space shuttle.[25] At the shuttle altitude of 200 km, $n_e \approx 10^5 cm^{-3}$ and B = 0.5 gauss so that $\omega_{pe}/\omega_{ce} = 3$ suggesting the electrons motion may not be one-dimensional. Furthermore, beam injection takes place at a local point while the return current can be drawn at any shuttle surface which is conducting. Simulations of such effects will require a two-dimensional model. Spacecraft charging and the limit of the current injected from a spacecraft must be determined self-consistently, including the electric field generated by the beam electrons.[23]

ACKNOWLEDGMENTS

The authors would like to thank Dr. H. Abe for his comments and interest in this work.

This work was supported by the U.S. Department of Energy Contract No. DE-AC02-76-CHO-3073, National Science Foundation Grant ATM-85-12512, and Air Force Grant F19628-85-K-0027.

REFERENCES

[1]J.R. Pierce, J. Appl. Phys. 19, 231 (1949).

[2]O. Buneman, Phys. Rev. 115, 503 (1959).

[3]R.J. Briggs, Electron-Stream Interaction with Plasma (MIT Press, Cambridge, Massachusetts, 1964).

[4]W.E. Drummond and D. Pines, Nucl. Fusion, Suppl. Pt. 3, 1049 (1962).

[5]A.A. Vedenov, E.P. Velikhov, and R.Z. Sagdeev, Nucl. Fusion 1, 82 (1961); suppl. 72, 465 (1962).

[6]B.B. Kadomtsev, Plasma Turbulence (Academic, New York, 1965), p. 15.

[7]W.E. Drummond, J.H. Malmberg, T.M. O'Neil, and J.R. Thompson, Phys. Fluids 13, 2422 (1970).

[8]T.M. O'Neil, J.H. Winfrey, and J.H. Malmberg, Phys. Fluids 14, 1204 (1971).

[9]V.D. Shapiro and V.I. Shevchenko, Nucl. Fusion, 12, 133 (1972).

[10]I.N. Onishchenko, A.R. Linetskii, N.G. Matsiborko, V.D. Shapiro, and V.I. Shevchenko, Soviet Phys. JETP Lett. 2, 281 (1970).

[11]N.G. Matsiborko, I.N. Onishchenko, V.D. Shapiro, and V.I. Shevchenko, Plasma Phys. 14, 591 (1972).

[12]K.V. Roberts and H.L. Berk, Phys. Rev. Lett. 19, 297 (1967).

[13]S. Kainer, J. Dawson, R. Shanny, and T. Coffey, Phys. Fluids 15, 493 (1972).

[14]H. Okuda, R. Horton, M. Ono, and K.L. Wong, Phys. Fluids 28, 3365 (1985).

[15]A.T. Lin and J.E. Rowe, Phys. Fluids 15, 166 (1972).

[16]H. Abe, O. Fukumasa, R. Itatani, and H. Naitou, Phys. Fluids 22, 310 (1979).

[17]A.T. Lin, J.M. Dawson, and M.Z. Caponi, Phys. Fluids 24, 1364 (1981).

[18]H. Okuda and M. Ashour-Abdalla, J. Geophys. Res. 88, 899 (1983).

[19]See, for example, A Survey of Phenomena in Ionized Gasses (International Atomic Energy Agency, Vienna, 1968), p. 109.

[20]Artificial Particle Beams in Space Plasma Studies edited by Bjorn Grandel (Plenum Press, New York, 1982).

[21]K.L. Wong, M. Ono, and G.A. Wurden, Rev. Sci. Instrum. 53, 409 (1982).

[22]J.D. Lindl and J.S. Degroot, Bull. Am. Phys. Soc. 17, 1045 (1972).

[23]H. Okuda and J.R. Kan, Phys. Fluids (in press).

[24]H. Okuda, Laser and Particle Beams (in press).

[25]T. Obayashi, N. Kawashima, K. Kuriki, M. Nagatomo, K. Ninomiya, S. Sasaki, M. Yamagisawa, I. Kudo, M. Ejiri, W.T. Roberts, C.R. Chappell, P.L. Reasoner, J.L. Burch, W.L. Taylor, P.M. Banks, P.R. Williamson, and O.K. Garriott, Science 225, 195 (1984).

FIGURE CAPTIONS

FIG. 1 Phase-space plots for the pulsed beam propagation at $\omega_{pe}t$ = 0(a), 30(b), 60(c), and 90(d). Case 1.

FIG. 2 Electric field structure at $\omega_{pe}t$ = 10(a), 30(b), 60(c), and 90(a). Case 1.

FIG. 3 Local velocity distributions at 4 bins at $\omega_{pe}t$ = 90. Case 1.

FIG. 4 Phase-space plots for the initial plateau distribution at $\omega_{pe}t$ = 0(a), 30(b), 60(c), and 100(d). Case 2.

FIG. 5 Electric field and local particle distributions at $\omega_{pe}t$ = 50(a), (b), and $\omega_{pe}t$ = 90(c), (d). Case 2.

FIG. 6 Electric field (a), ambient electron density (b), beam electron phase space (c), and ambient electron phase space (d) at $\omega_{pe}t$ = 10. Case 3.

FIG. 7 Electric field (a), ambient electron density (b), beam electron phase space (c), and ambient electron phase space (d) at $\omega_{pe}t$ = 20. Case 3.

FIG. 8 Electric field (a), ambient electron density (b), beam electron phase space (c), and ambient electron phase space (d), at $\omega_{pe}t$ = 50. Case 3.

FIG. 9 Electric field (a), ambient electron density (b), beam electron phase space (c), and ambient electron phase space (d), at $\omega_{pe}t$ = 100. Case 3.

FIG. 10 Total electron velocity distribution at $\omega_{pe}t$ = 80. Case 3

FIG. 11 Power spectrum of the electric field measured at a location x = 512Δ. Case 3.

FIG. 12 Phase-space plots for the beam (a), (c), and ambient electrons, (b), (d) at $\omega_{pe}t$ = 50 and 100. L = 1024Δ. Case 4.

FIG. 13 Electric field (a), ambient electron density (b), beam electron phase space (c), and ambient electron phase space (d) at $\omega_{pe}t$ = 10. Only the region of $0 \leq x \leq 256\Delta$ is shown. Case 5.

FIG. 14 Electric field (a), ambient electron density (b), beam electron phase space (c), and ambient electron phase space at $\omega_{pe}t$ = 50. L = 512Δ. Case 5.

FIG. 15 Total electron velocity distribution and beam phase space at $\omega_{pe}t$ = 20 (a), (b), and at $\omega_{pe}t$ = 50 (c), (d), Case 6.

FIG. 16 Electric field (a), ambient electron density (b), beam electron phase space (c), and ambient electron phase space at $\omega_{pe}t$ = 25. L = 1024Δ. Case 7.

FIG. 17 Beam (a) and ambient electron (b) phase space at $\omega_{pe}t \approx 50$. Case 7.

FIG. 18 Phase space plots for the beam (a), (c) and ambient electrons (b), (d) at $\omega_{pe}t = 25$ and 45. $L = 2048\Delta$. Case 8.

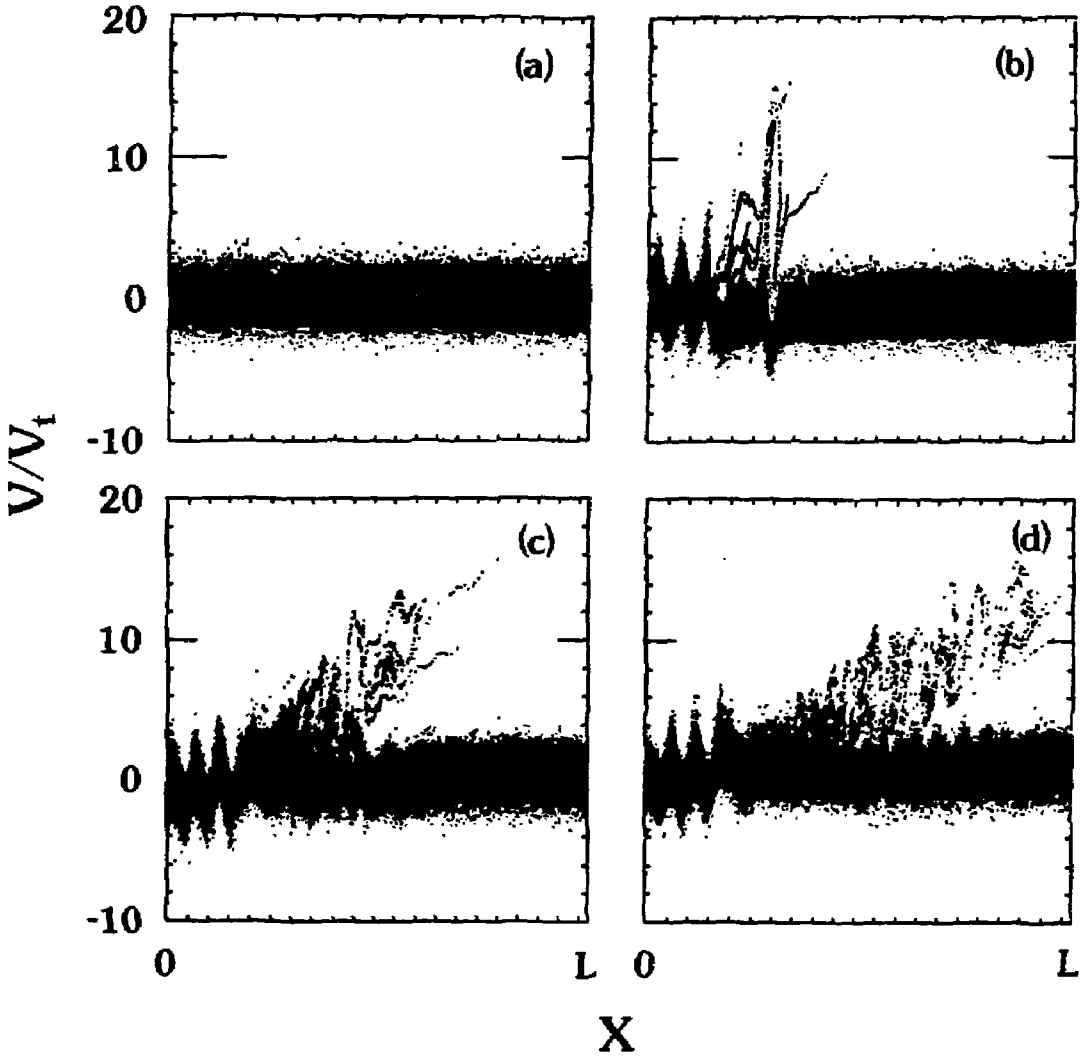

Fig. 1

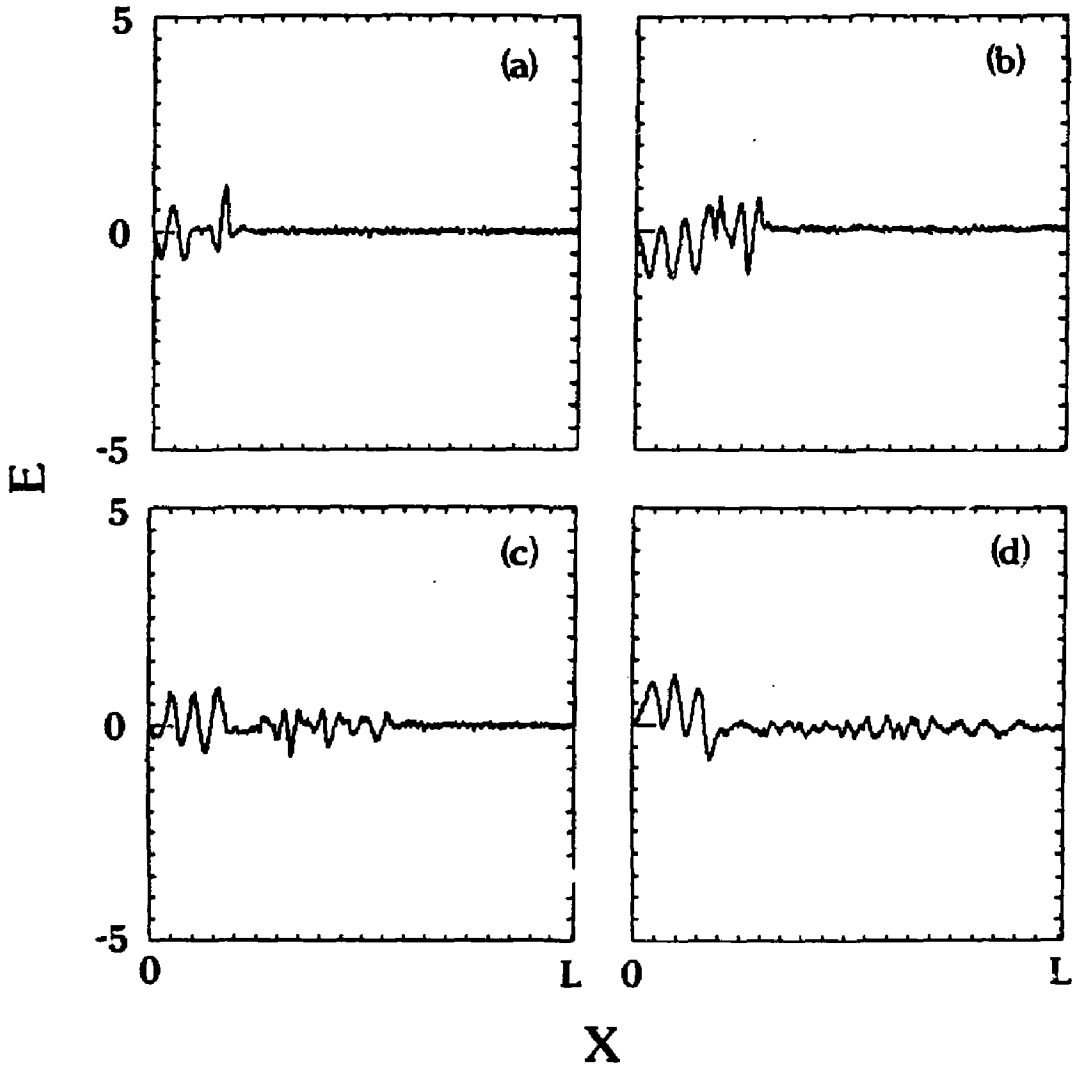

Fig. 2

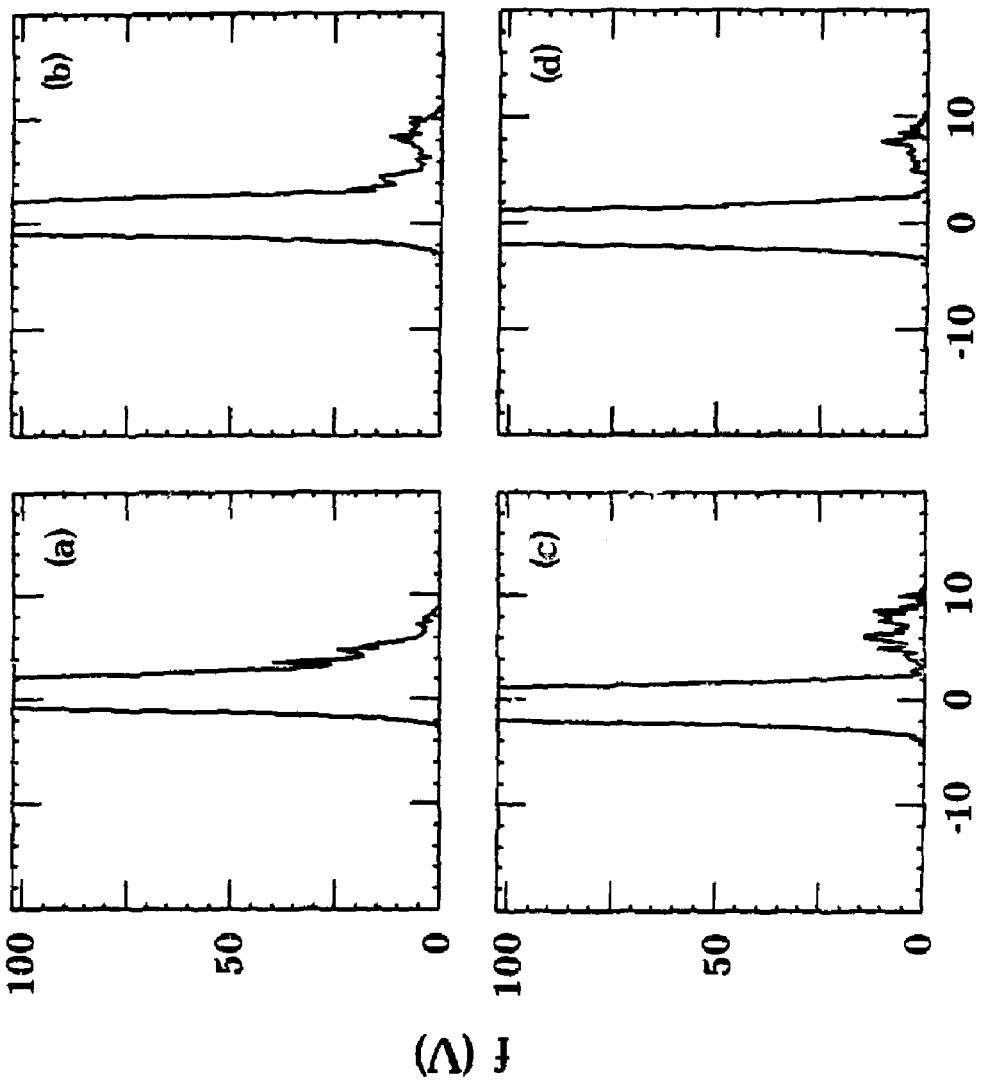

Fig. 3

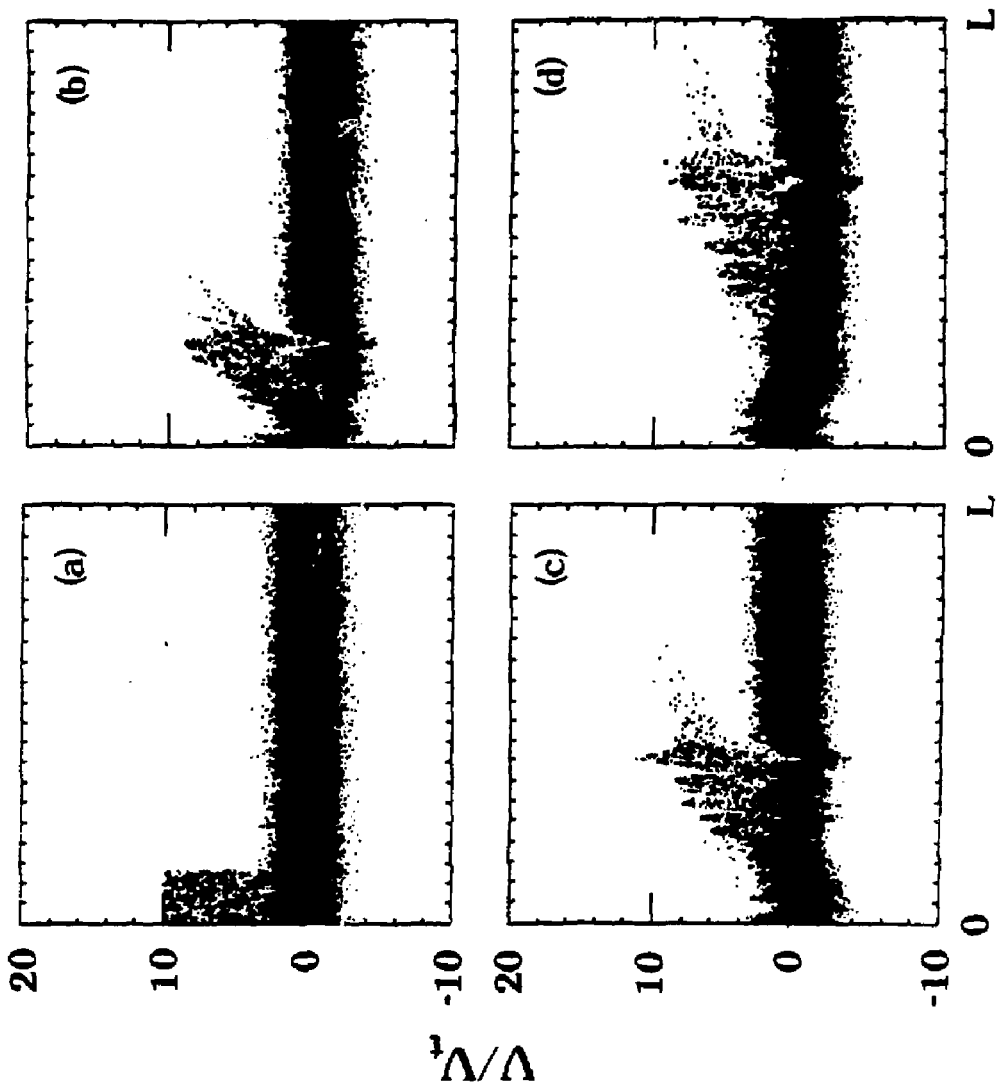

Fig. 4

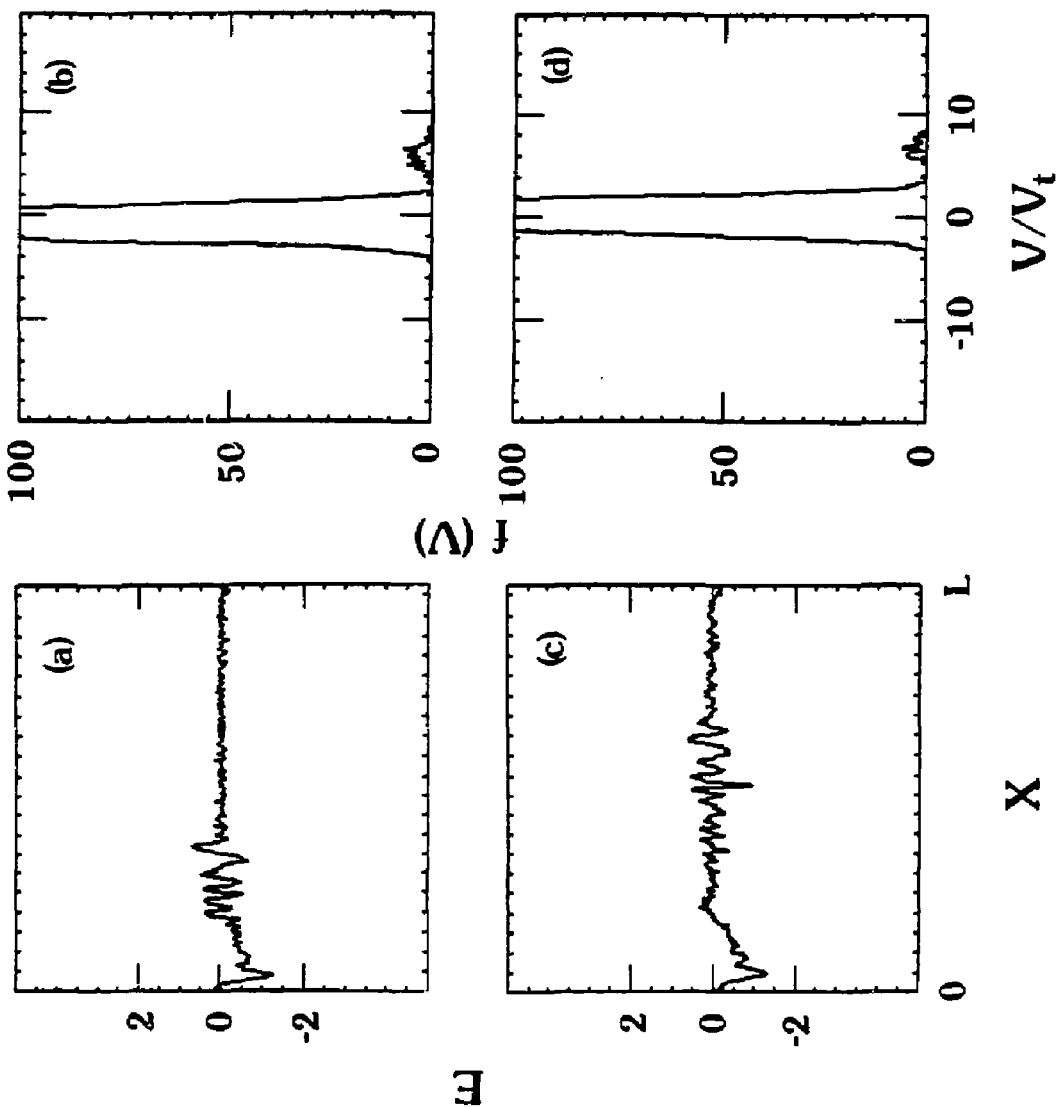

Fig. 5

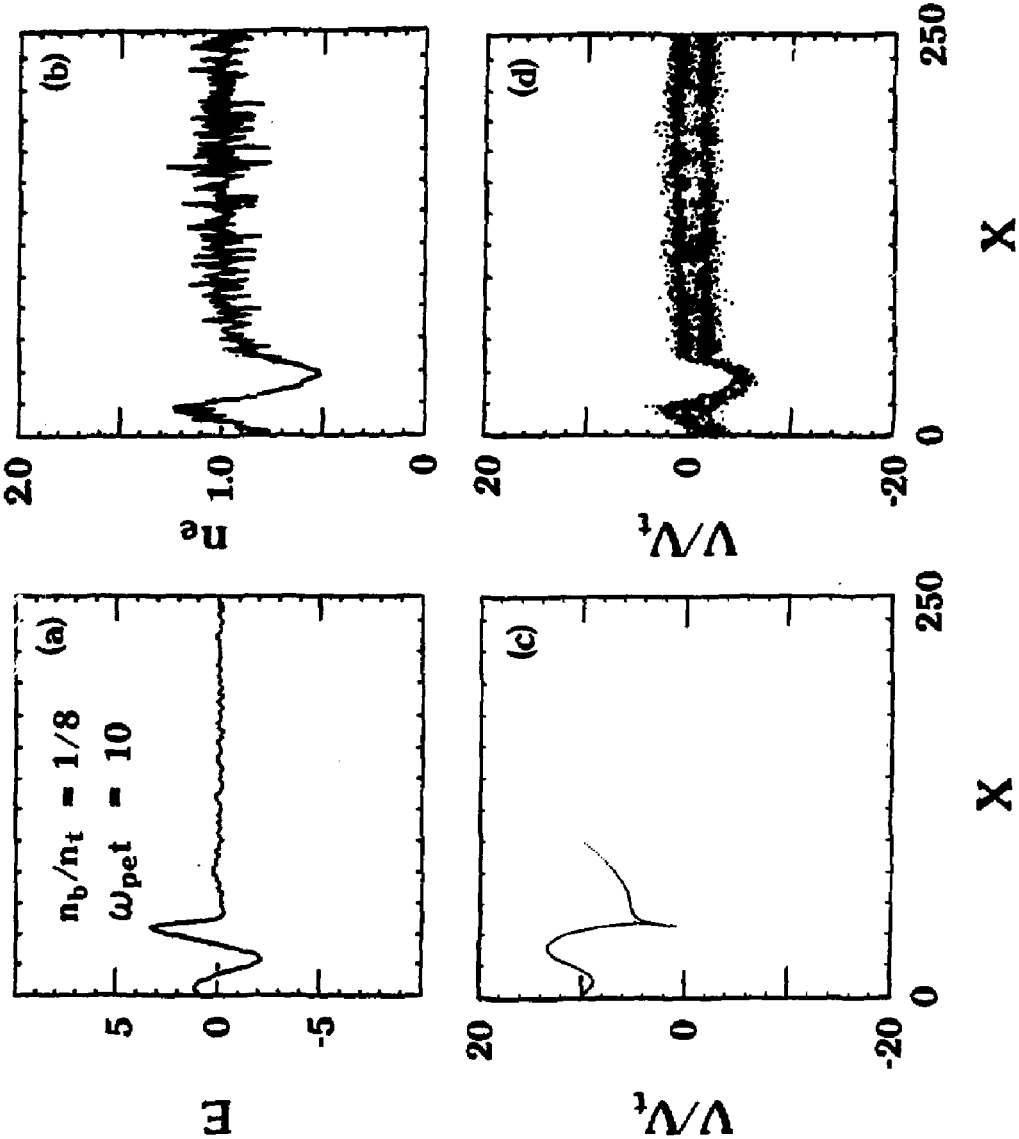
(a)
n_b/n_t = 1/8
$\omega_{pe}t$ = 10
E
5
0
-5
(b)
n_e
2.0
1.0
0
(c)
V/V_t
20
0
-20
0
250
X
(d)
V/V_t
20
0
-20
0
250
X

Fig. 6

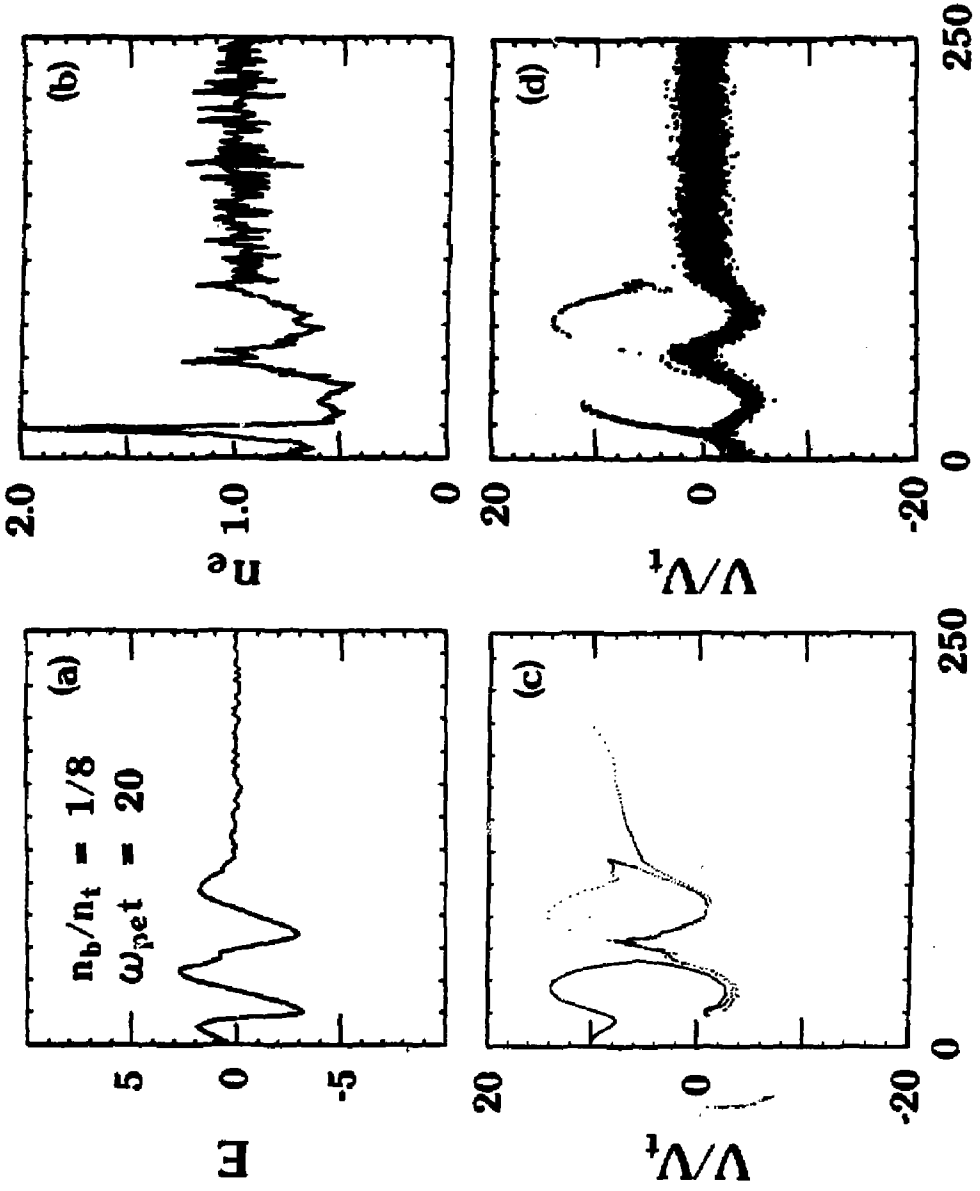
(a)
n_b/n_t = 1/8
$\omega_{pe}t$ = 20
E
5
0
-5
(b)
n_e
2.0
1.0
0
(c)
V/V_t
20
0
-20
(d)
V/V_t
20
0
-20
0
250
X
0
250
X

Fig. 7

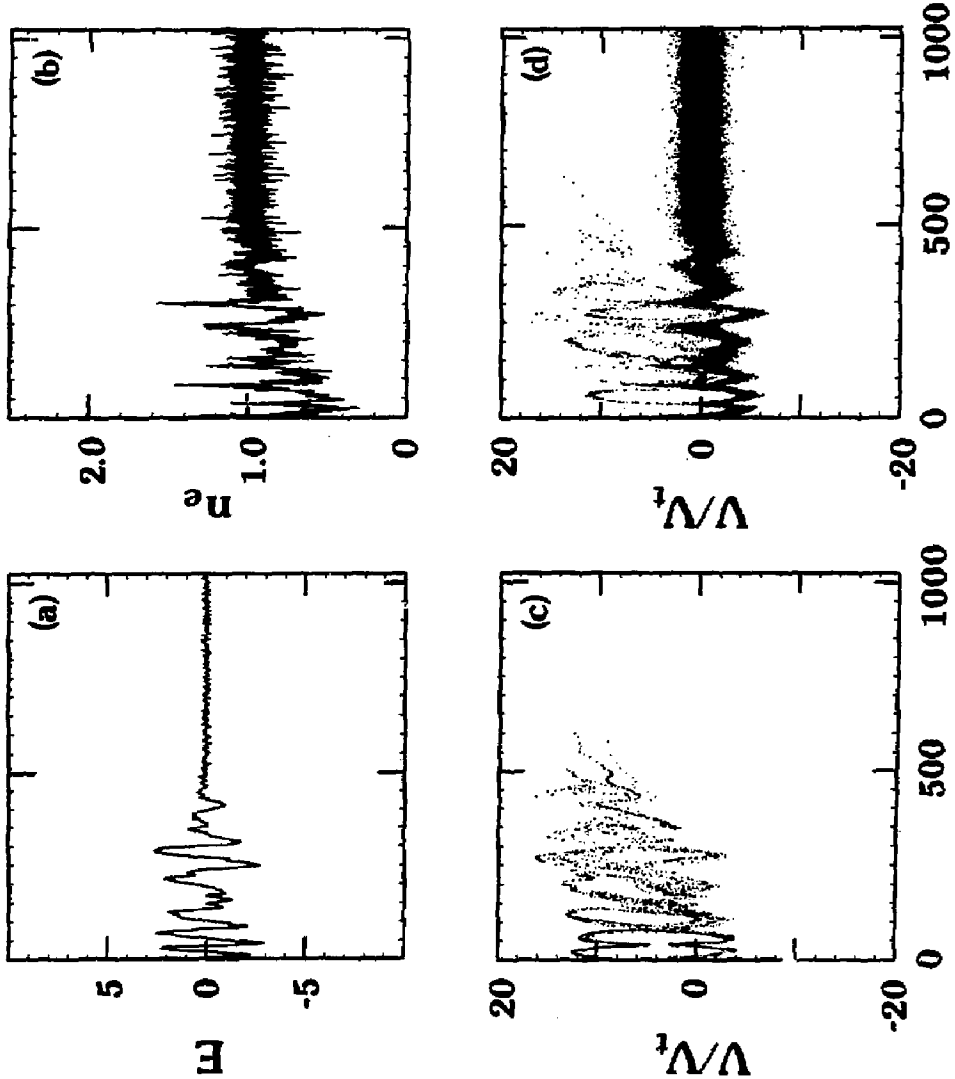

Fig. 8

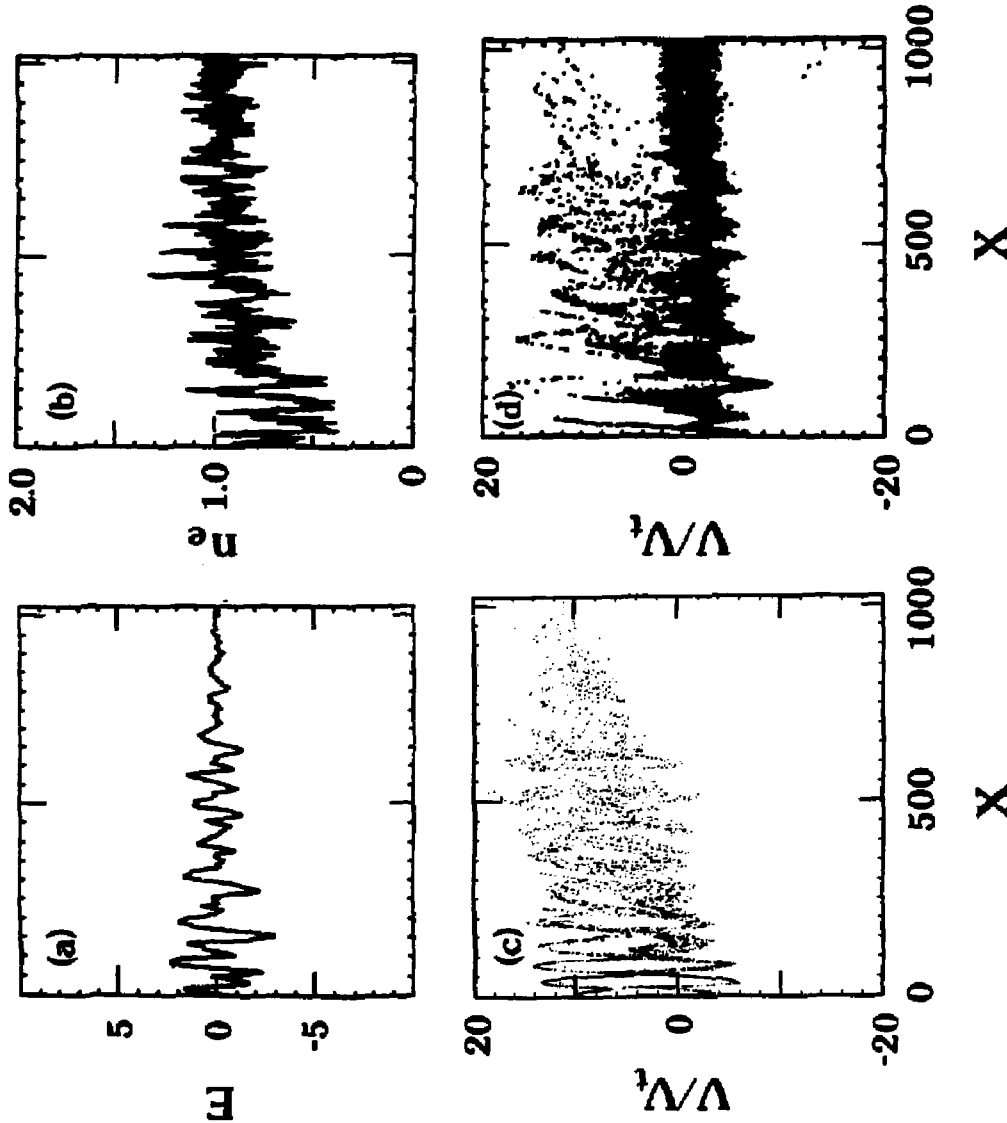

Fig. 9

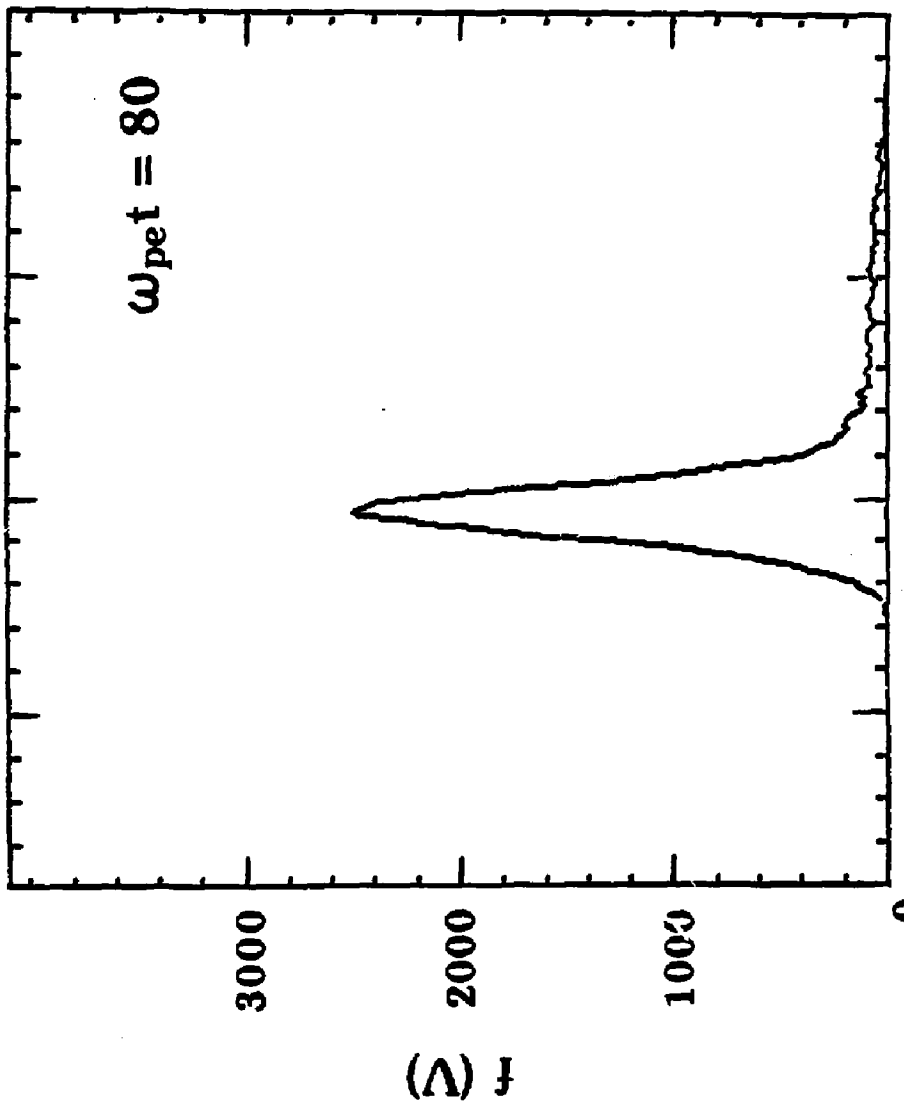

Fig. 10

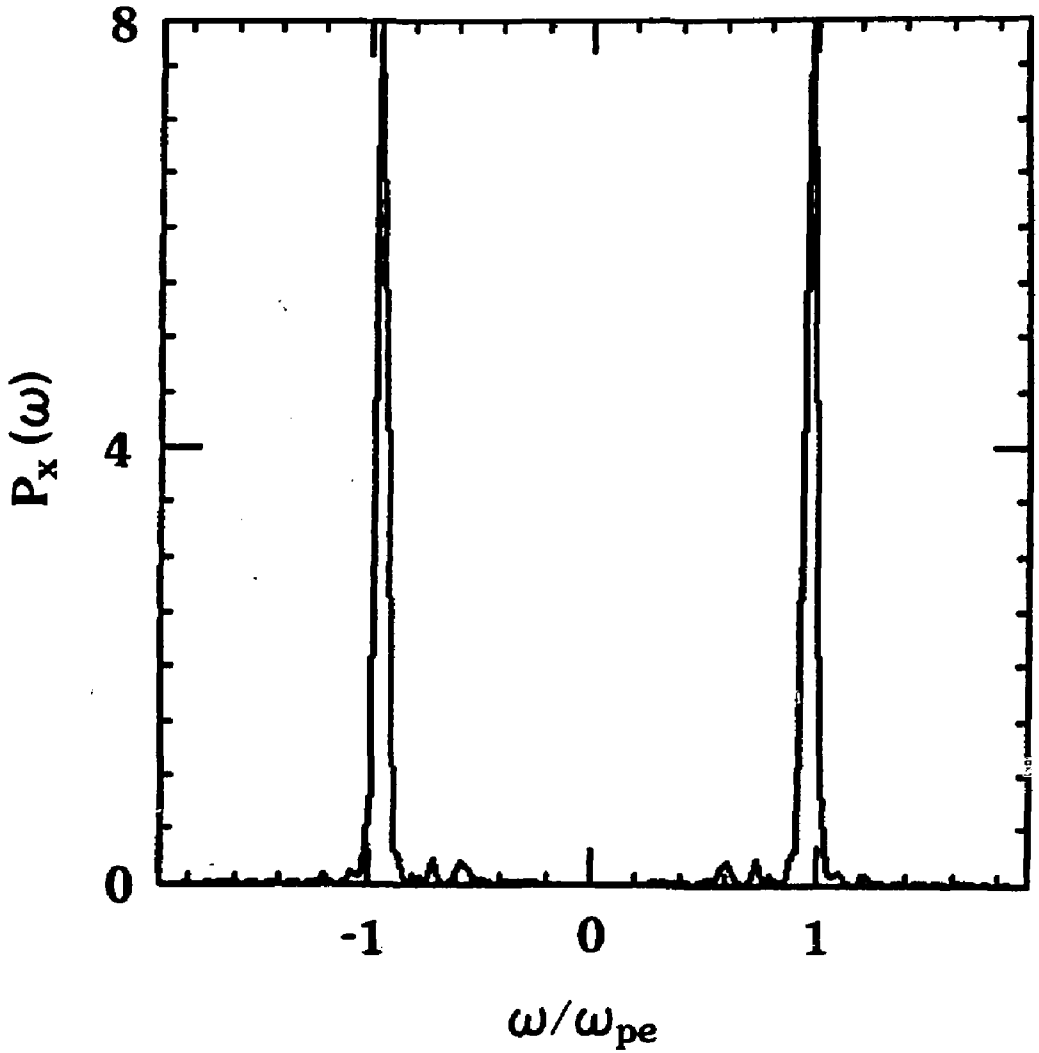

Fig. 11

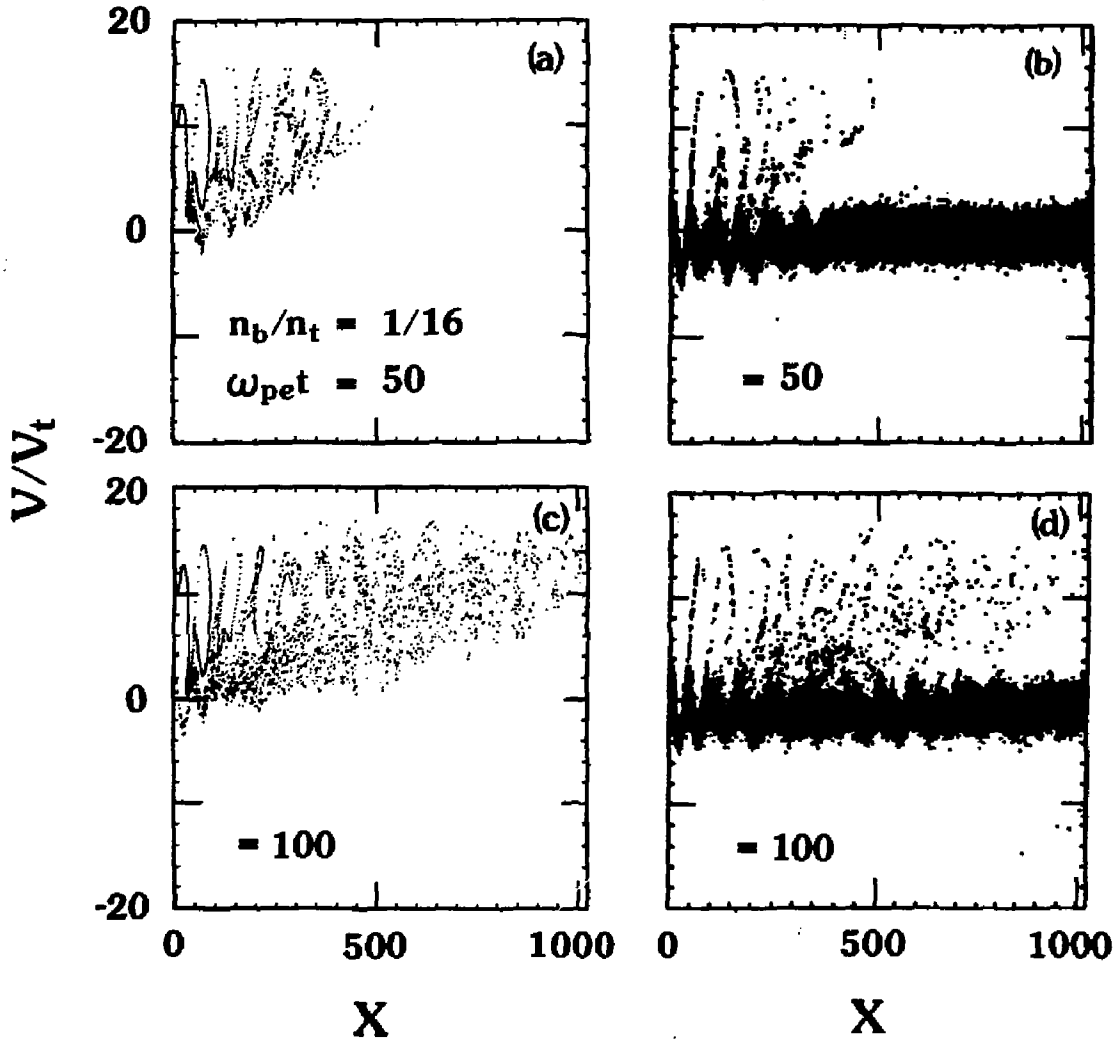

Fig. 12

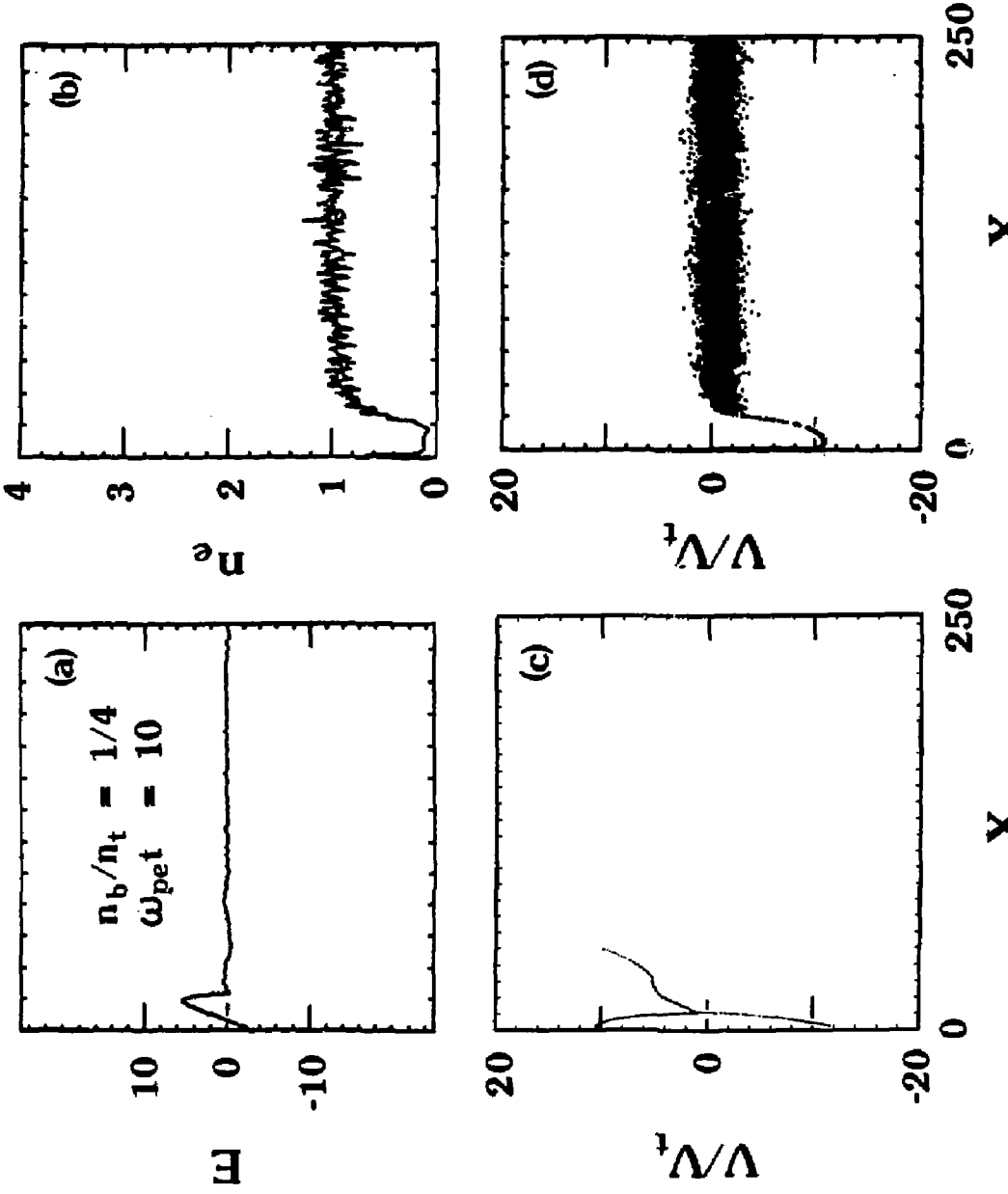
(a)
n_b/n_t = 1/4
$\omega_{pe}t$ = 10
E
10
0
-10
(b)
n_e
4
3
2
1
0
(c)
V/V_t
20
0
-20
0
250
X
(d)
V/V_t
20
0
-20
0
250
X

Fig. 13

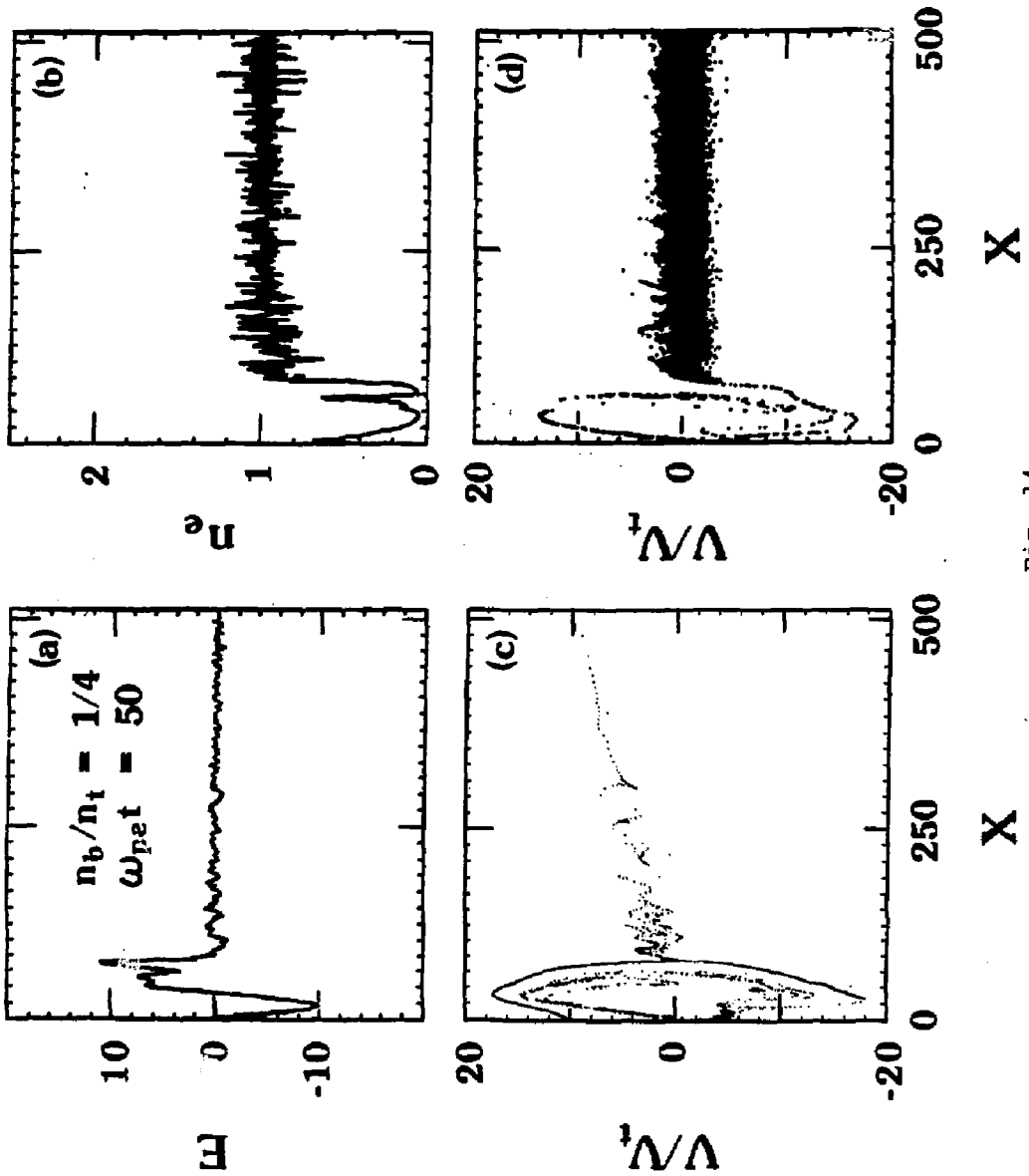

Fig. 14

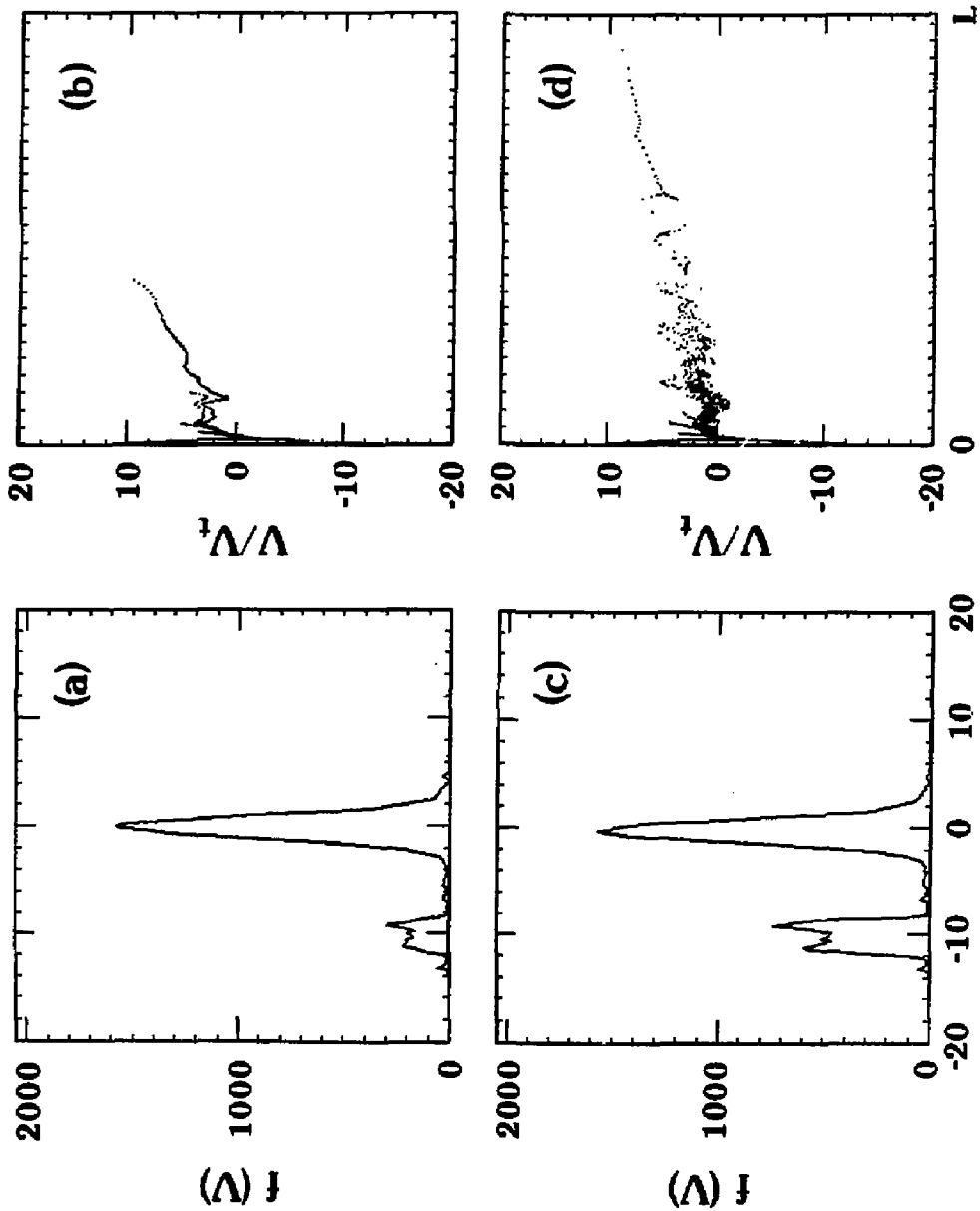

Fig. 15

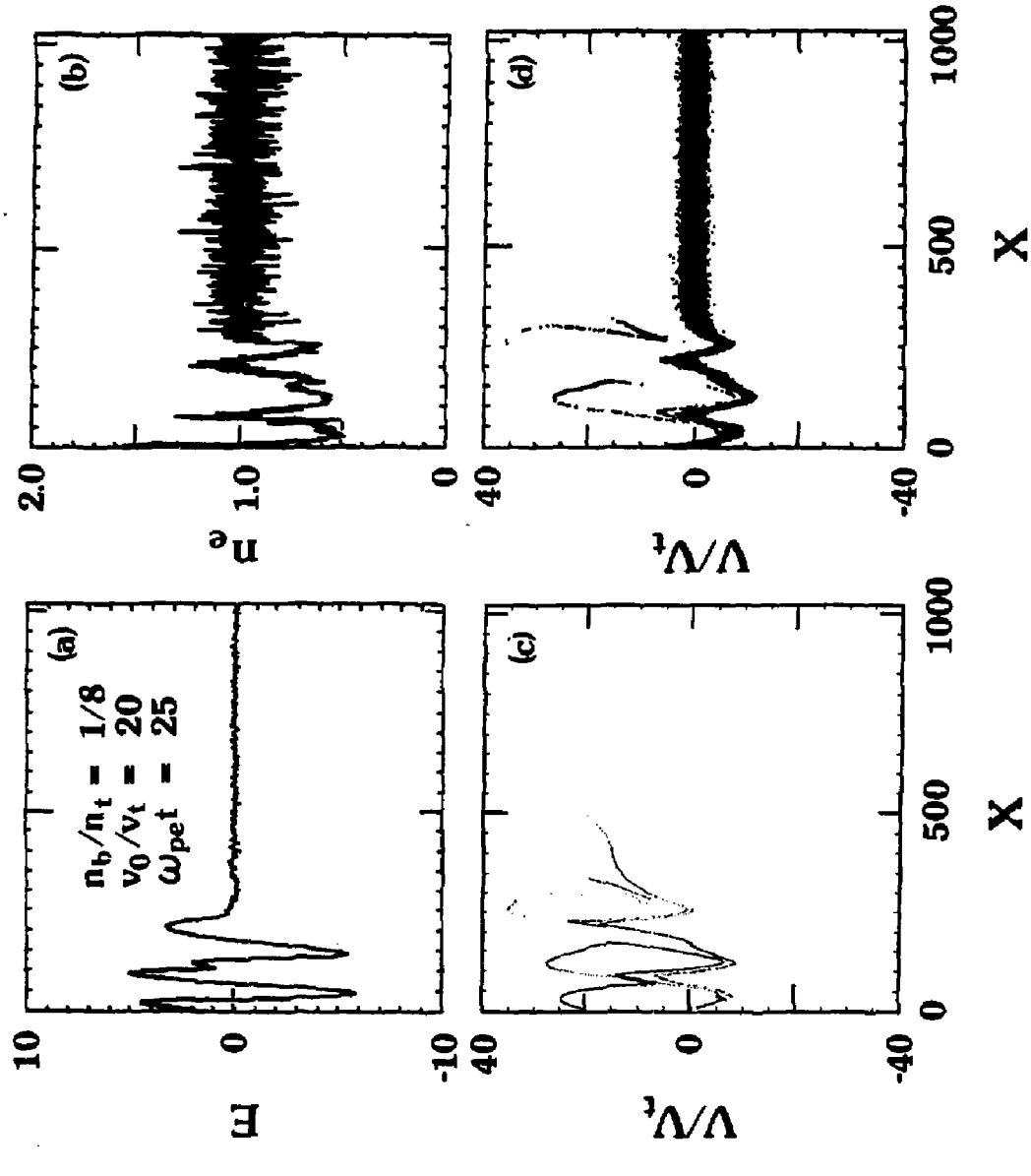
(a)
n_b/n_t = 1/8
v_0/v_t = 20
$\omega_{pe}t$ = 25
E
10
0
-10
(b)
n_e
2.0
1.0
0
(c)
V/V_t
40
0
-40
(d)
V/V_t
40
0
-40
0
500
1000
X
0
500
1000
X

Fig. 16

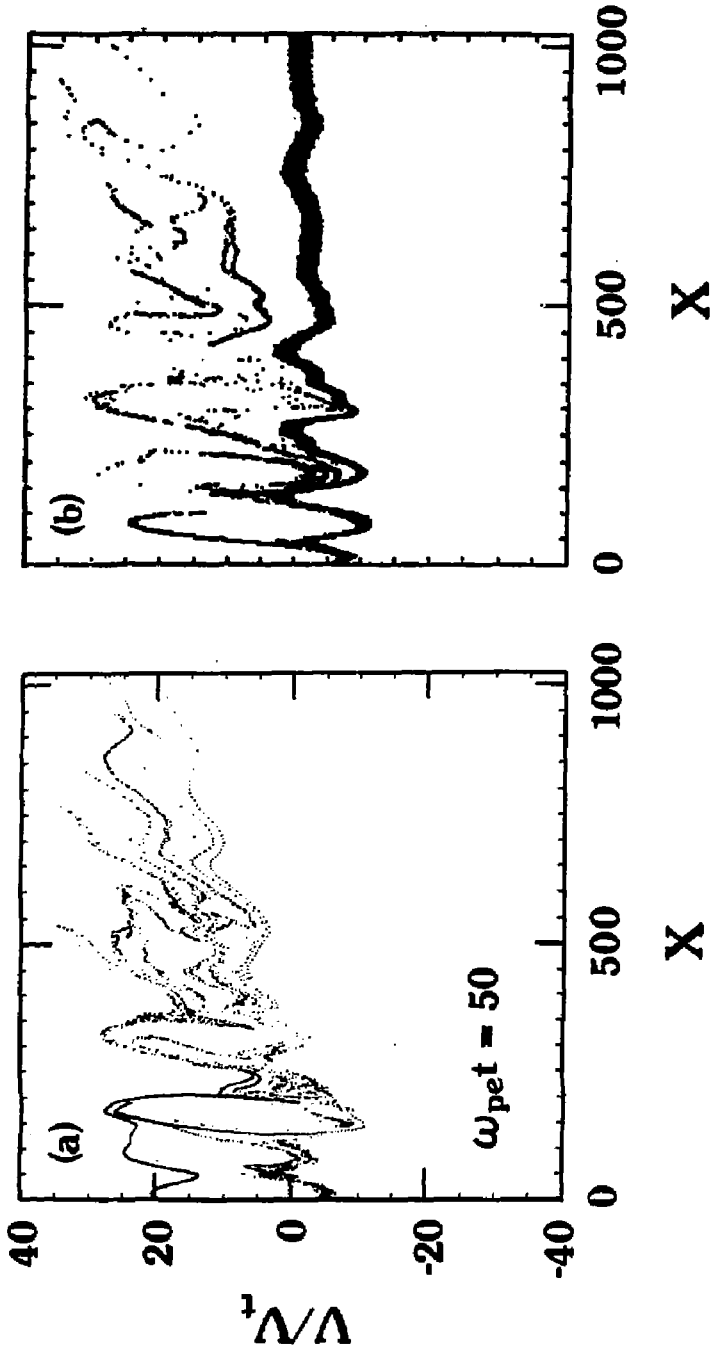

Fig. 17

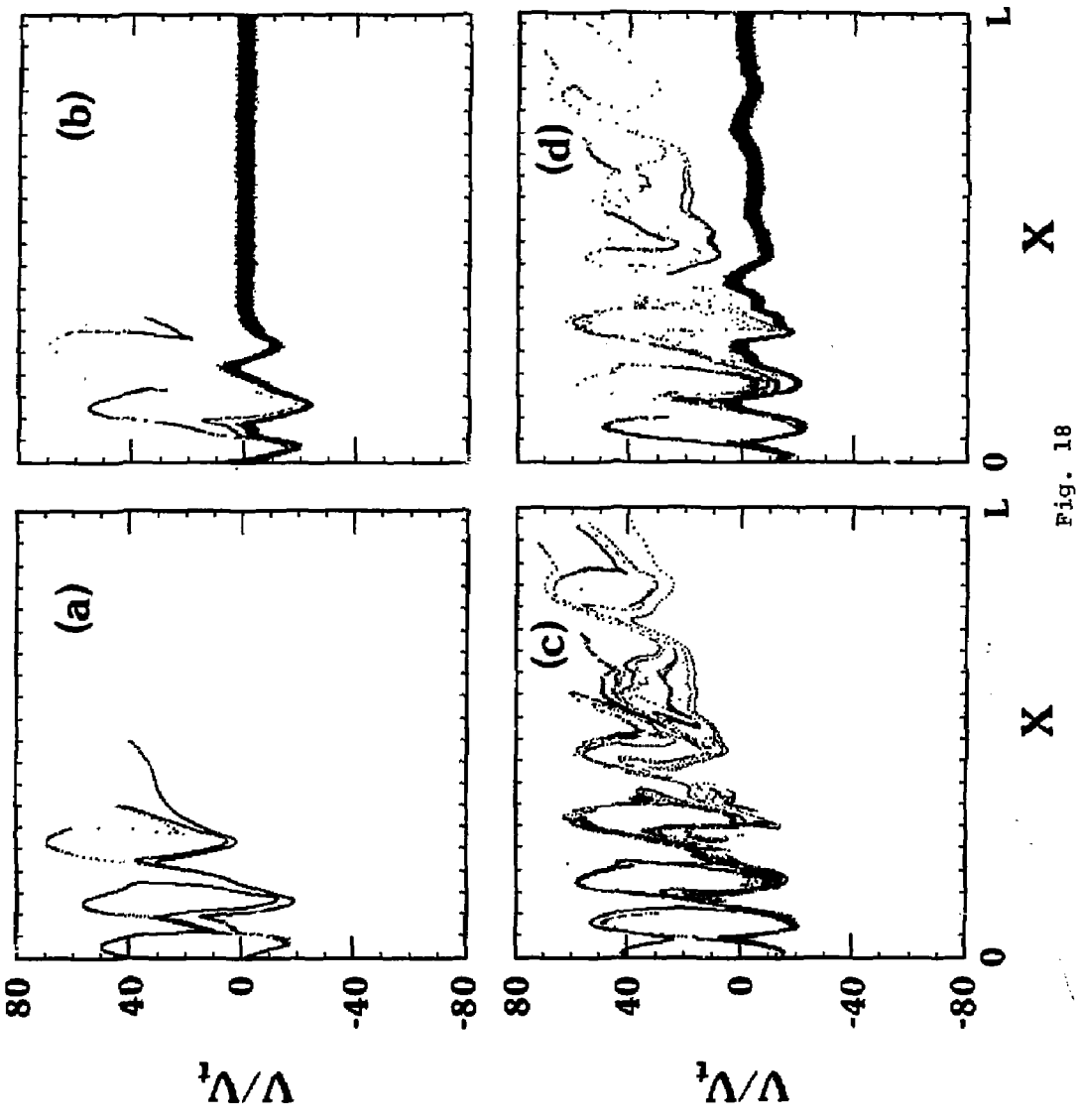

Fig. 18

EXTERNAL DISTRIBUTION IN ADDITION TO UC-20

Plasma Res Lab, Austra Nat'l Univ, AUSTRALIA
Dr. Frank J. Paoloni, Univ of Wollongong, AUSTRALIA
Prof. I.R. Jones, Flinders Univ., AUSTRALIA
Prof. M.H. Brennan, Univ Sydney, AUSTRALIA
Prof. F. Cap, Inst Theo Phys, AUSTRIA
M. Goossens, Astronomisch Instituut, BELGIUM
Prof. R. Boucique, Laboratorium voor Natuurkunde, BELGIUM
Dr. D. Palumbo, Dg XII Fusion Prog, BELGIUM
Ecole Royale Militaire, Lab de Phys Plasmas, BELGIUM
Dr. P.H. Sakanaka, Univ Estadual, BRAZIL
Lib. & Doc. Div., Instituto de Pesquisas Espaciais, BRAZIL
Dr. C.R. James, Univ of Alberta, CANADA
Prof. J. Teichmann, Univ of Montreal, CANADA
Dr. H.M. Skarsgard, Univ of Saskatchewan, CANADA
Prof. S.R. Sreenivasan, University of Calgary, CANADA
Prof. Tudor W. Johnston, INRS-Energie, CANADA
Dr. Hannes Barnard, Univ British Columbia, CANADA
Dr. M.P. Bachynski, MPB Technologies, Inc., CANADA
Chalk River, Nucl Lab, CANADA
Zhengwu Li, SW Inst Physics, CHINA
Library, Tsing Hua University, CHINA
Librarian, Institute of Physics, CHINA
Inst Plasma Phys, Academia Sinica, CHINA
Dr. Peter Lukac, Komenskeho Univ, CZECHOSLOVAKIA
The Librarian, Culham Laboratory, ENGLAND
Prof. Schatzman, Observatoire de Nice, FRANCE
J. Radet, CEN-BP6, FRANCE
JET Reading Room, JET Joint Undertaking, ENGLAND
AM Dupas Library, AM Dupas Library, FRANCE
Dr. Tom Musi, Academy Bibliographic, HONG KONG
Preprint Library, Cent Res Inst Phys, HUNGARY
Dr. R.K. Chhajlani, Vikram Univ, INDIA
Dr. B. Dasgupta, Saha Inst, INDIA
Dr. P. Kaw, Physical Research Lab, INDIA
Dr. Phillip Rosenau, Israel Inst Tech, ISRAEL
Prof. S. Cuperman, Tel Aviv University, ISRAEL
Prof. G. Rostagni, Univ DI Padova, ITALY
Librarian, Int'l Ctr Theo Phys, ITALY
Miss Ciella De Palo, Assoc EURATOM-ENEA, ITALY
Biblioteca, del CNR EURATOM, ITALY
Dr. H. Yamato, Toshiba Res & Dev, JAPAN
Direc. Dept. Lg. Tokamak Dev, JAERI, JAPAN
Prof. Nobuyuki Inoue, University of Tokyo, JAPAN
Research Info Center, Nagoya University, JAPAN
Prof. Kyoji Nishikawa, Univ of Hiroshima, JAPAN
Prof. Sigeru Mori, JAERI, JAPAN
Prof. S. Tanaka, Kyoto University, JAPAN
Library, Kyoto University, JAPAN
Prof. Ichiro Kawakami, Nihon Univ, JAPAN
Prof. Satoshi Itoh, Kyushu University, JAPAN
Dr. D.I. Choi, Adv. Inst Sci & Tech, KOREA
Tech Info Division, KAERI, KOREA
Bibliotheek, Fom-Inst Voor Plasma, NETHERLANDS
Prof. B.S. Liley, University of Waikato, NEW ZEALAND
Prof. J.A.C. Cabral, Inst Superior Tecn, PORTUGAL
Dr. Octavian Petrus, ALI CUZA University, ROMANIA
Prof. M.A. Hellberg, University of Natal, SO AFRICA
Dr. Johan de Villiers, Plasma Physics, Nucor, SO AFRICA
Fusion Div. Library, JEN, SPAIN
Prof. Hans Wilhelmson, Chalmers Univ Tech, SWEDEN
Dr. Lennart Stenflo, University of UMEA, SWEDEN
Library, Royal Inst Tech, SWEDEN
Centre de Recherchesen, Ecole Polytech Fed, SWITZERLAND
Dr. V.T. Tolok, Kharkov Phys Tech Ins, USSR
Dr. D.D. Ryutov, Siberian Acad Sci, USSR
Dr. G.A. Eliseev, Kurchatov Institute, USSR
Dr. V.A. Glukhikh, Inst Electro-Physical, USSR
Institute Gen. Physics, USSR
Prof. T.J.M. Boyd, Univ College N Wales, WALES
Dr. K. Schindler, Ruhr Universitat, W. GERMANY
ASDEX Reading Rm, IPP/Max-Planck-Institut fur Plasmaphysik, F.R.G.
Nuclear Res Estab, Julich Ltd, W. GERMANY
Librarian, Max-Planck Institut, W. GERMANY
Bibliothek, Inst Plasmaforschung, W. GERMANY
Prof. R.K. Janev, Inst Phys, YUGOSLAVIA